EBioMedicine 27 (2018) 27–39

Contents lists available at ScienceDirect

EBioMedicine

journal homepage: www.ebiomedicine.com

Research Paper

T Cells Primed by Live Mycobacteria Versus a Tuberculosis Subunit Vaccine Exhibit Distinct Functional Properties

Thomas Lindenstrøm [a,*], Albanus Moguche [b], Mie Damborg [a], Else Marie Agger [a], Kevin Urdahl [b], Peter Andersen [a,*]

[a] Department of Infectious Disease Immunology, Statens Serum Institut, Denmark
[b] Center for Infectious Disease Research, Seattle, USA

ARTICLE INFO

Article history:
Received 18 August 2017
Received in revised form 22 November 2017
Accepted 5 December 2017
Available online 7 December 2017

Keywords:
M. tuberculosis
Natural immunity
Vaccination
T cell priming & differentiation
Lung homing

ABSTRACT

Despite inducing strong T cell responses, *Mycobacterium tuberculosis* (Mtb) infection fails to elicit protective immune memory. As such latently infected or successfully treated Tuberculosis (TB) patients are not protected against recurrent disease. Here, using a mouse model of aerosol Mtb infection, we show that memory immunity to H56/CAF01 subunit vaccination conferred sustained protection in contrast to the transient natural immunity conferred by Mtb infection. Loss of protection to re-infection in natural Mtb memory was temporally linked to an accelerated differentiation of ESAT-6- and to a lesser extent, Ag85B-specific CD4 T cells in both the lung parenchyma and vasculature. This phenotype was characterized by high KLRG1 expression and low, dual production of IFN-γ and TNF. In contrast, H56/CAF01 vaccination elicited cells that expressed low levels of KLRG1 with copious expression of IL-2 and IL-17A. Co-adoptive transfer studies revealed that H56/CAF01 induced memory CD4 T cells efficiently homed into the lung parenchyma of mice chronically infected with Mtb. In comparison, natural Mtb infection- and BCG vaccine-induced memory CD4 T cells exhibited a poor ability to home into the lung parenchyma. These studies suggest that impaired lung migratory capacity is an inherent trait of the terminally differentiated memory responses primed by mycobacteria/mycobacterial vectors.

1. Introduction

CD4 T cells play a central role for protective immunity against tuberculosis (TB) as underscored by several human studies and animal models of TB (Caruso et al., 1999; Green et al., 2013; Lawn et al., 2009). Although the precise nature and full spectrum of effectors by which CD4 T cells mediate protection remains elusive (Gallegos et al., 2011; Orme et al., 2015; Sakai et al., 2016), CD4 T cell derived IFN-γ stands out as a key cytokine essential for protection against *Mycobacterium tuberculosis* (Mtb) infection (Green et al., 2013). Nevertheless, boosting the Ag-specific IFN-γ response is not sufficient to confer protection against TB, as highlighted by the recent failure of the MVA85A efficacy trial, which failed to enhance protection beyond BCG despite its immunogenicity (Tameris et al., 2013). Furthermore, there is increasing evidence that high levels of IFN-γ may even be detrimental in some circumstances (Kagina et al., 2010; Leal et al., 2001; Sakai et al., 2016). These insights have further fueled the search for better correlates of protection, and risk in humans (Berry et al., 2010; Fletcher et al., 2016; Petruccioli et al., 2016; Zak et al., 2016) as well as studies in animal models aiming to unravel the precise nature of a protective T cell response to Mtb infection (Moguche et al., 2015; Orme et al., 2015; Reiley et al., 2010; Sakai et al., 2014; Torrado et al., 2015). A number of recent studies in the mouse model have made it clear that protective responses are connected to Mtb-specific CD4 T cells that have the ability to migrate into the lung parenchyma (Moguche et al., 2015; Sakai et al., 2014; Woodworth et al., 2016) where they can make cognate interactions with the infected macrophages (Srivastava & Ernst, 2013). These studies also demonstrate that Mtb infections in mice drive disparate populations of CD4 T cells that differ in their anatomical localization within the lung. One population is confined to the lung vasculature, whereas the other can be found within the parenchyma. The intravascular subset is comprised of CD4 T cells skewed towards terminal differentiation characterized by high expression of the transcription factor T-bet, the inhibitory receptor KLRG1 and the fractalkine receptor CX3CR1. These cells have a limited capacity to mediate control of Mtb infection, but produce significant amounts of Th1 related cytokines like IFN-γ and TNF. In contrast, Mtb-specific CD4 T cells in the lung parenchyma represent cells with a much lower differentiation status characterized by expression of the transcription factor Bcl-6, the inhibitory receptor PD-1, the co-stimulatory molecule ICOS and the chemokine

* Corresponding authors at: Department of Infectious Disease Immunology, Statens Serum Institut, Artillerivej 5, 81/348, DK-2300 Copenhagen S, Denmark.
E-mail addresses: thi@ssi.dk, pa@ssi.dk (T. Lindenstrøm).

https://doi.org/10.1016/j.ebiom.2017.12.004

receptor CXCR3. These cells produce lower levels of the Th1 effector cytokines but produce relatively higher amounts of IL-2 and mediate superior protection than their intravascular counterparts (Moguche et al., 2015; Sakai et al., 2014; Torrado et al., 2015). These findings mirror data gained within the field of the cellular therapy of cancer, where central memory T cells play a crucial role for immune protection (Crompton et al., 2015; Klebanoff et al., 2005). Here, experiments employing adoptive cells therapy (ACT) have shown improved persistence of T_{CM} over T_{Eff} and revealed that efficient migration into tumor target tissue (deep lesional tumor infiltration) is a particular asset of T cells with a low degree of differentiation and associated with improved prognosis (Busch et al., 2016; Crompton et al., 2015; Sackstein et al., 2017).

The novel insights into the importance of T cell attributes during Mtb infections are all derived from mice with fulminant infections, which do not cover the full spectrum of disease manifestation in humans and in particular may differ from low-grade infections or situations that mimic latency. Humans latently infected or successfully treated for active TB are often not protected against relapse (Bryant et al., 2013; Guerra-Assuncao et al., 2015; Luzze et al., 2013) or re-infection (De Boer & Van Soolingen, 2000; Verver et al., 2005), even in the face of an initial strong Mtb-specific Th1 effector and memory response (Cardoso et al., 2002; Joosten et al., 2016; Lindestam Arlehamn et al., 2013; Scriba et al., 2017). The dissection of this conundrum is essential to understand the essence of natural immunity as well as learn from its potential shortcomings. A number of murine models of post-primary Mtb (Henao-Tamayo et al., 2012; Jung et al., 2005; Kamath & Behar, 2005; Mollenkopf et al., 2004) have addressed memory responses and the protection provided against secondary infections. These models differ in terms of infection route, extent and administration of chemotherapy, length of resting period prior to secondary infection as well as duration of the primary infection. Despite these differences, a common denominator seems to be that natural memory does indeed provide significant albeit short lived protection (Henao-Tamayo et al., 2012). Although secondary responses are anamnestic in nature (Kamath & Behar, 2005), they do not appear to differ qualitatively relative to primary responses and their protective benefit is primarily based on the accelerated nature of the response (Jung et al., 2005). One of our early studies showed that the protection achieved against a short-term 4 week challenge was mediated primarily by less-differentiated, Mtb-specific T_{CM}-like CD4 T cells (Andersen & Smedegaard, 2000). In light of the recent insights on T cell differentiation status and lung localization, we wanted to address the stability of CD4 T cell differentiation state long-term after priming by Mtb infection compared to subunit vaccination with H56/CAF01. Additionally we wanted to evaluate the extent to which this differentiation stability impacted lung homing capacity and ability to mediate sustained protection against Mtb challenge.

2. Materials and Methods

2.1. Mice

Age and sex matched C57BL/6 mice and CB6F1 mice (Envigo; Netherlands) were housed in BSL-3 facilities at Statens Serum Institut and acclimatized for 1 week prior to experimentation. All experimental procedures were approved by the local ethical committee and conducted in accordance with the regulations of the Danish Ministry of Justice and animal protection committees under permit 2014-15-2934-01065 and in compliance with European Union Directive 2010/63/EU. Wild type C57BL/6 and congenically marked B6 mice strains (B6·PL-Thy1^{a}/cyJ and B6·SJL-Ptprc^{a}Pep3^{b}BoyJ) were purchased from Jackson laboratories (Bar Harbor, ME). Mice were bred and maintained under specific pathogen-free conditions at the Center for Infectious Disease Research Institute (CIDR) and experimental procedures involving animals were approved by the IACUC.

2.2. Immunizations/Generation of Mtb Immune Memory Mice

H56 memory mice were generated by subcutaneous (s.c.) injection of respective mice at the base of the tail with three bi-weekly doses of 5 μg recombinant H56 in CAF01 (DDA/TDB; 250/50 μg dose) in a total volume of 200 μl. Mtb memory mice were established using a method described by Henao-Tamayo et al. (Henao-Tamayo et al., 2012). Briefly, mice were infected with low dose (100 cfu) aerosol Mtb Erdman strain (TMC107, ATCC) using a Biaera Aero MP aerosol system. Starting at 6 weeks post-infection mice were treated for 12 weeks with Isoniacid/Rifabutin (INH/RIF) treatment administered through the drinking water as previously described (Hoang et al., 2013). BCG immunization was achieved by a single s.c. dose of 1×10^6 BCG Pasteur administered in a volume of 200 μl.

2.3. Mtb-Infection and CFU Enumeration

Primary infection and/or aerosol challenge of memory mice was performed using a Biaera exposure system controlled via AeroMP software. Virulent *M. tuberculosis* Erdman (TMC 107, ATCC) or H37Rv was grown to log-phase in Sauton medium (BD Pharmingen) enriched with 0.5% sodium pyruvate, 0.5% glucose, and 0.2% Tween 80. The log-phase bacteria was aliquoted and stored at −80 °C. At the day of infection, the bacteria were thawed and sonicated for 5 min to remove clumps. Additional clumps were removed by dispersing bacteria through a syringe. After washing, the bacteria were diluted to 0.5×10^6 CFU/ml in 1× PBS. The inoculum was aerosolized for inhalation in the Biaera Aero MP aerosol system calibrated to deliver an average dose of 50–100 CFU/mice. Infection dose was confirmed by sacrificing a cohort of 2 mice immediately after aerosol infection, homogenizing the whole lungs and plating in Middlebrook 7h11 plates for bacterial growth. Post infection, treatment or immunization, lung bacterial burdens were determined in left lung lobes from individual mice. Lungs were homogenized using M-tubes and Miltenyi AutoMACS Dissociator (Miltenyi, Germany). Homogenates were serially diluted in 1× PBS and plated onto Middlebrook 7H11 agar plates. The plates were dried to remove excessive liquid and moisture and incubated at 37 °C for ~3 weeks before CFU enumeration.

Similar to what has been reported in the literature (Rosenthal et al., 2012; Scanga et al., 1999), a small fraction of mice cleared from Mtb infection by 12 weeks INH/RIF treatment experienced regrowth starting approximately 3 months after end of treatment (EoT). However this relapse rate remained relatively stable (~15%) when Mtb memory mice were followed up until almost 1½ year after EoT (Supplementary Table 1). We assured that all mice included in the phenotypic characterization were culture-negative (detection limit < 10 CFU/lungs) throughout the 6 months resting period (week 40) by control plating serial dilutions of lung homogenates of left lung lobes from all mice included in the characterization.

2.4. In Vivo Intravascular Labeling of T Cells

At day of experiment, mice were injected intravenously with phycoerythryn (PE), Allophycocyanin (APC) or Fluorescein isothiocynate (FITC) labeled antibodies. 1–2 μg of antibody was used per mouse in a total volume of 200 μl. Some of the antibodies used for intravascular labeling were against CD45.2, CD90.2, or CD4. For antibodies against CD4, clone RM4–4 that does not block the other clones (RM4-5 and Gk1.1) was used. All the antibodies were purchased from Biolegend, San Diego, CA. Three minutes after antibody injection, mice were euthanized and lung single cell suspensions prepared as described below.

2.5. Preparation of Single Cell Suspensions

Lungs aseptically removed from euthanized mice and were left unperfused in cases, where the in vivo intravascular labeling technique was employed (Figs. 2–6). In remaining cases, where iv-labeling was

not used (Supplementary Figs. 1–3), isolated lungs were perfused-with cold RPMI prior to being processed. Isolated lungs were transferred into Miltenyi C tubes containing HEPES/RPMI buffer supplemented with Collagenase (Roche/Sigma) and eventually 10 U/ml of DNAse (Sigma). The lungs were subsequently homogenized and digested for 30–45 min at 37 °C and passed through cell strainers (BD Biosciences). After washing, the cells were re-suspended RPMI media containing 5% FBS and stored on ice until use. Spleen and lymph nodes were kept at 4 °C until being directly processed through cell strainers followed by two washes in media. After last wash, cells were stained directly for MHC II tetramers and surface markers or stimulated for ICS analysis.

2.6. Tetramer and Surface Staining of Lung Single Cell Suspensions

Tetramers (ESAT-$6_{4\text{-}17}$:I-A^b, Ag85$B_{280\text{-}294}$:I-A^b and TB10.$4_{70\text{-}84}$:I-A^d) conjugated to APC, PE or BV421 and corresponding negative controls (hCLIP:I-A^b and hCLIP:I-A^d) were provided by the NIH tetramer facility (Atlanta, USA). Single cells suspensions were stained with appropriately diluted MHC-II tetramers (ESAT-6 and TB10.4: 1:100; Ag85B: 1:50 or 1:100). MHC-II tetramer staining was done either at room temperature for 1 h or for 30 min at 37 °C. Surface staining with respective antibodies was done at 4 °C for 30 min. The antibodies were appropriately diluted in a buffer containing Fc block and 5% FBS and 1× PBS. Some of the antibodies used included anti-CD3-PerCp (Cat# 561089 RRID:AB_10584323), anti-CD4-BV510 (Cat# 563106 RRID:AB_2687550), anti-CD44-BV786 (IM7), anti-ICOS (CD278)-BV421 or –PE (Cat# 552146 RRID:AB_394349), anti-KLRG1- BV711 (2F1) – all BD Biosciences, anti-PD-1 (CD279)-BV605 (BioLegend Cat# 135220, RRID:AB_2562616), anti-CXCR3 (CD183)-PerCP-Cy5.5 (Thermo Fisher Scientific Cat# 45-1831-82, RRID:AB_1210699), and anti-CX3CR1-PE (Goat IgG, R&D Systems). Dead cells were excluded using the fixable viability dye eF780 (eBioscience). After staining, cells were analyzed using the BD LSRFortessa flowcytometer. All gate boundaries for cell surface markers were based on fluorescence-minus-one controls (FMOs) and subsequent flow cytometry analysis performed using FlowJo software v.X (Tree Star, Ashland, OR, USA). An overview of gating strategy is depicted in Supplementary Fig. 4.

2.7. Enrichment of Tetramer and or Low Frequency Donor Cells

In the spleens, lymph nodes and lungs (when too few cells were expected) when required, MHC II tetramer + cells and or donor cells were enriched according to the protocol described by Moon et al. (Moon et al., 2007). In brief, single cell suspensions from spleens or lungs were stained with fluorochrome conjugated tetramers and or respective congenic marker as described above. After staining the cells were washed and re-suspended in FACS buffer followed by addition anti-fluorochrome magnetic microbeads (Miltenyi Biotech) and incubated at 4 °C for 30 min. Some of the anti-magnetic beads used were anti-PE, anti-APC and anti-FITC. After washing, tetramer and/or congenic marker binding cells were enriched over an LS column (Miltenyi Biotech) as per manufacturer's instructions. Positive tetramer binding cells were collected and eluted after removal of the magnet and were subsequently stained for cell surface markers as described above and analyzed by flow cytometry. Gating strategy for the Mtb:H56 co-adoptive transfer studies is depicted in Supplementary Fig. 5.

2.8. In Vitro Stimulation and Intracellular Cytokine Staining

Intracellular staining was done as previously described (Lindenstrøm et al., 2013). Briefly, 1–2 × 10^6 cells were stimulated in vitro in V-bottom 96-well plates at 37 °C in RPM1 with 10% FBS and 10 μg/ml Brefeldin A. The cells were stimulated with 2 μg/ml ESAT-$6_{1\text{-}15}$ peptide, 1 μg/ml anti-CD28 (clone 37.51) or anti-CD49d (clone 9C10-MFR4.B) for 5–6 h. Cells were washed with FACS buffer (PBS containing 0.1% sodium azide and 1% FCS) followed by staining with surface antibodies as necessary. Fixation and permeabilization was carried out using the Cytofix/Cytoperm kit (BD Biosciences) as per manufacturer's instructions followed by intracellular staining with fluorochrome conjugated antibodies against the respective cytokines. Some of the cytokines antibodies used were anti–IFN-γ PE-Cy7 (BD Biosciences Cat# 557649 RRID:AB_396766), anti–TNF–PE (BD Biosciences Cat# 554419 RRID:AB_395380), IL-2–APC–Cy7 (BD Biosciences Cat# 560547 RRID:AB_1727544) and IL-17A–PerCP–Cy5.5 (Thermo Fisher Scientific Cat# 45–7177-82 RRID:AB_925753).

2.9. Adoptive Transfer Experiments

For co-adoptive transfer of H56 and Mtb memory CD4 T cells into chronically infected recipients, donor CD4 T cells were isolated by negative selection using the EasySep mouse CD4 T cell enrichment kit (Stemcell Technologies). CD4 T cells were isolated to 93–95% purity from spleens and draining lymph nodes (tracheobronchial (Mtb) and inguinal (H56), respectively) taken from resting H56 and Mtb memory mice at week 49–50 post immunization/chemo. Prior to donor cell harvest, Mtb memory mice were put on an additional INH/RIF treatment period 10 weeks to assure that none of them had experienced relapse. Purified memory CD4 T cells were pooled from 10 donors within each group of memory mice. For tracking, respective congenic markers were used or cells were differentially stained for 8–10 min with 10 μM Cell Proliferation Dye eFluor450 (H56 memory cells) and 5 μM Cell Proliferation Dye eFluor670 (Mtb memory cells). The proliferation dyes were quenched with 1xPBS containing 20% FBS followed by washing and re-suspension in 1xPBS. The cells were mixed in a ~1:1 ratio and co-adoptively transferred into the same recipient mice (the equivalent of one of each donor mice/each recipient mice) infected with Mtb for 34 weeks prior. Subsequent analysis of the mixed donor-cells revealed that the actual ratio of I-A^b:ESAT-6-specific CD4 T cells transferred was 1.67:1 H56 to Mtb memory cells with <3% dead cells (corresponding to 63% H56 & 37% Mtb memory; see Supplementary Fig. 5A). H56 memory comparison with BCG memory was done by transfer into recipient mice infected with Mtb for ~10 weeks. 18–20 hour post transfer, recipient mice were injected with respective antibodies for intravascular labeling and single cell suspensions from the lung prepared as described above.

2.10. Statistical Analysis

Prism software (v.7 GraphPad, San Diego, CA) was used to perform all statistical analyses. CFU data and numbers of ESAT-6 Tet + cells were log-transformed to normalize variance before analysis. Statistical significance was determined with either One-way ANOVA with Tukey's multiple comparison test or Two-way ANOVA with appropriate post hoc tests. *t*-test was used for simple comparisons between two groups. Statistical methods and results are described in the figure legends. Number of experimental repeats and number of mice are likewise stated in each figure legend.

3. Results

3.1. ESAT-6-specific CD4 T Cells Primed by Mtb Infection Are more Differentiated than those Primed by H56/CAF01

In order to study the natural CD4 T cell memory response to Mtb without the influence of ongoing bacterial replication and high antigen load, we employed a mouse model of latent Mtb infection that results in uncultivable bacteria (Henao-Tamayo et al., 2012). Following INH/RIF treatment bacterial loads declined precipitously and by the end of the treatment regimen and up to 72 weeks post treatment, no bacteria was detected in the majority of infected mice. We also monitored the number and phenotype of ESAT-6-specific CD4 T cells for ~40 weeks, covering a period prior to, during and after treatment. All mice included

in the phenotypic characterization during the post-treatment period were culture-negative (detection limit <10 CFU/lungs). The infection/treatment schedule was aligned to H56/CAF01 vaccinations by comparing Mtb memory responses at end of treatment (EoT/week 12) with H56 vaccine-promoted memory responses at 12 weeks post last immunization (Fig. 1A). In order to provide time for full memory transition and study long-term memory, CD4 T cell responses in both Mtb treated and H56/CAF01 vaccinated mice were followed for at least 40 weeks (Fig. 1A). In the Mtb treated mice, bacterial clearance led to a steady contraction of ESAT-6-specific CD4 T cells in the spleen when enumerated using ESAT-$6_{4\text{-}17}$: I-A^b tetramers coupled with magnetic enrichment. From week 12 onwards, a similar contraction of ESAT-6-specific CD4 T cells was found in the spleen of H56 vaccinated mice. Indeed, the number of memory ESAT-6-specific CD4 T cells in the spleen of Mtb treated mice was equivalent to those of H56 vaccinated mice at week 40 ($P > 0.05$) (Fig. 1B). Despite the absence of cultivable bacteria as well as a significant resolution of inflammation by week 12/EoT, we found that a large fraction of ESAT-$6_{4\text{-}17}$:I-A^b specific CD4 T cells in the spleen expressed KLRG1 with some cells also expressing PD-1 or ICOS; either alone or in conjunction with KLRG1. This was in contrast to ESAT-6 memory cells in the spleen of H56 memory mice, of which the vast majority of cells expressed PD-1 and ICOS with a complete absence of KLRG1 expression (Fig. 1C). At week 40 after treatment start, memory CD4 T cells in the spleens had reached a more quiescent state with low levels of PD-1 and ICOS expression and substantial expression of CXCR3 in both H56 and Mtb treated memory mice (Fig. 1C). A population of KLRG1 expressing ESAT-6-specific cells was still detectable in the spleen of Mtb memory mice at week 40 (Fig. 1C). The contraction and progression to memory phenotype was also reflected in the lungs of Mtb infected and treated mice, where the largest contraction of ESAT-6 specific cells occurred during the first 6 weeks of chemotherapy and with a clear population of KLRG1 expressing cells remaining at week 40 (Supplementary Fig. 1). Overall, Mtb primed memory responses therefore remained more differentiated than after H56/CAF01 imprinting (Fig. 1C & Supplementary Fig. 2).

3.2. Mtb Memory Provides Early but Transient Protection to Infection

We next evaluated protection against Mtb challenge in H56/CAF01 vaccinated and in Mtb treated mice rested ~½ year after EoT. Memory mice (H56 and Mtb) plus age-matched uninfected controls were exposed to an aerosol infection and protective efficacy evaluated for 20-weeks. At 2 weeks post challenge, both sets of memory mice harbored significantly lower bacterial burdens in the lung (~1 Log_{10}, $P < 0.01$)

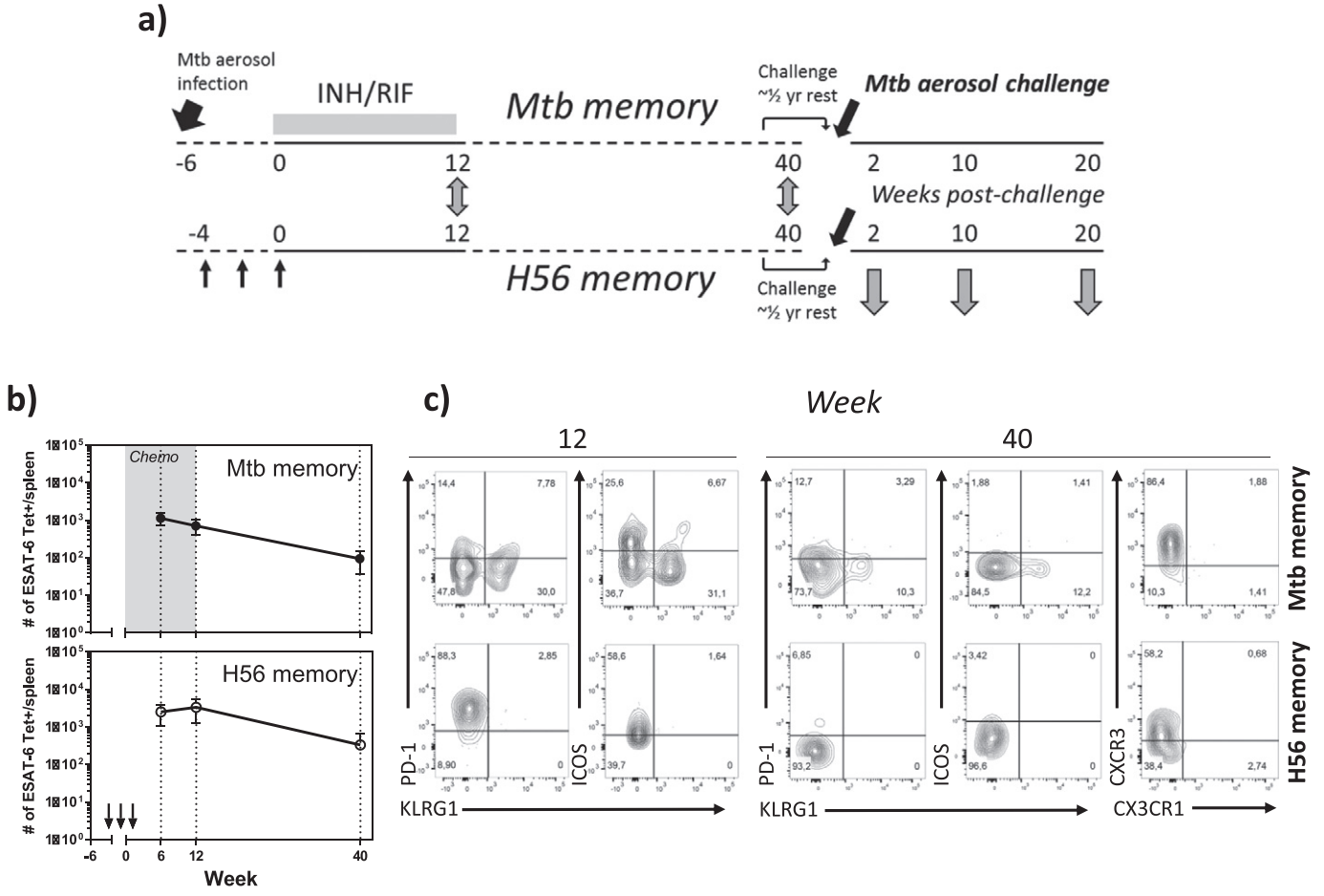

Fig. 1. Resting memory cells after a cleared Mycobacterium tuberculosis infection show a higher degree of differentiation than memory cells primed by H56/CAF01 vaccination. A) Schematic overview of the experimental outline. C57BL/6 mice, aerosol infected for 6 weeks, were subjected to a 12 week Isoniacid/Rifabutin (INH/RIF) treatment. ESAT-6 specific memory cells in the spleen were phenotypically characterized at week 12/End of Treatment (EoT) by ESAT-$6_{4\text{-}17}$:I-A^b pulldown using magnetic bead-based tetramer enrichment and compared to E6 memory responses 12 week post three s.c. immunizations with H56/CAF01, each spaced by two weeks. ESAT-6 specific memory cells in the spleen were similarly characterized and compared between the two groups of resting memory mice at week 40 after immunization/start of treatment. In order to study protective efficacy, H56 and Mtb memory mice were allowed to rest for half a year and then aerosol infected with Mtb Erdman. Protective efficacy was evaluated at week 2, 10 and 20 after challenge. B) The number of ESAT-$6_{4\text{-}17}$-specific CD4 T cells in the spleen was determined by Tetramer pulldown in Mtb (upper panel) and H56 (lower panel) memory mice at week 6, 12 and 40. Symbols, mean ± s.d. of 3–4 mice per time point. For Mtb memory mice, the experiment was repeated twice at week 6 and once at week 12 and 40. For H56 mice, the experiment was repeated twice at week 6 and 12 and once for week 40. C) Representative flow cytometry plots depicting KLRG1, PD-1, ICOS and CXCR3 (wk 40) expression by ESAT-6 tetramer-binding CD4 T cells in the spleen of Mtb (upper panels) and H56 (lower panels) memory mice at week 12 and 40.

compared to the controls (Fig. 2A). However, immune protection by natural Mtb memory rapidly declined and was completely lost by 10 weeks post challenge. In contrast, H56/CAF01 vaccination provided sustained protection that despite a narrowed protective window after week 10 of challenge, was still statistically significant up to 20 weeks post infection (Fig. 2A, 0.5 Log_{10} reduction over saline controls $P < 0.05$, difference between H56 and Mtb memory ns).

As lung parenchymal CD4 T cells have been associated with protection to Mtb in mice (Moguche et al., 2015; Sakai et al., 2014; Woodworth et al., 2016), we enumerated and compared the phenotypes of secondary effector T cells in the lung parenchyma and vasculature of Mtb versus H56 memory mice. Using ESAT-6_{4-17}:I-A^b tetramer staining together with intravenous (iv) anti-CD45 administration in order to differentiate cells in the lung vasculature (iv+) from cells within the lung parenchyma (iv−), we showed that both Mtb and H56 memory mice had small but equivalent ESAT-6-specific CD4 T cells in the lung vasculature (iv+) prior to infection (Fig. 2B). These numbers increased in both groups after challenge, but with no significant differences between Mtb and H56 memory mice during the course of infection (Fig. 2B). In contrast, prior to challenge resting Mtb memory mice had higher, though non-significant, numbers of ESAT-6-specific CD4 T cells in the lung parenchyma (iv−) compared to the H56 memory mice (Fig. 2C, time 0 ns). However at 2 weeks post challenge, both sets of mice had nearly equivalent numbers of ESAT-6-specific CD4 T cells in the lung parenchyma (Fig. 2C). This indicated enhanced expansion and/or recruitment of cells to the lung parenchyma in especially H56 memory mice. Indeed, the quantitative change in cell numbers within the parenchyma from onset of infection to two weeks post challenge was 1000 fold in H56 memory vs. controls, in contrast to a 10-fold change for Mtb memory (Fig. 2C). ESAT-6-specific CD4 T cells in the saline control groups progressively increased and were at par with the memory mice at 20 weeks post infection (Fig. 2C).

3.3. Secondary Effectors in the Lungs of H56 Memory Mice are Dominated by IL-2- and IL-17A-producing CD4 T Cell Subsets

We next sought to investigate qualitative differences in secondary effector T cell responses in Mtb and H56 memory mice after Mtb challenge. Based on a link between KLRG1-cells and production of IL-2 and IL-17 (Lindenstrøm et al., 2013; Moguche et al., 2015; Woodworth et al., 2016), we evaluated the connection between cytokine expression and tissue localization. Using the intravascular labeling technique, IL-2-production was found to be a key characteristic for H56 memory mice in both lung parenchyma and vasculature. Significantly, a majority of CD4 T cells in the lung parenchyma of H56 memory mice were comprised of triple cytokine (IFN-γ, IL-2 and TNF) producing cells, whereas most CD4 T cells in Mtb memory and naïve mice produced IFN-γ and TNF and completely lacked TNF and IL-2 co-producing cells likewise observed in H56 memory mice (Fig. 3). Hence, <10% of the ESAT-6-specific CD4 T cells in the iv+ compartment were found to express IL-2 in Mtb memory mice, whereas ~25% of the cells in the parenchyma were capable of producing IL-2. In H56 memory mice, for comparison, as much as 75% of the cytokine-producers within the lung parenchyma were positive for IL-2 in any combination (Fig. 3). In addition, H56/CAF01 vaccinated mice had a significant fraction of parenchymal CD4 T cells expressing IL-17A, a cytokine that was barely detectable in Mtb memory or naïve mice (Fig. 3).

3.4. Loss of Protection in Mtb Memory Mice Correlates With Increased Differentiation of Mtb-specific CD4 T Cells in the Lung

T cells with a low to intermediary state of differentiation along the Th1 axis have been shown to be highly protective in mouse models which have been linked to their superior capacity to home to the lung parenchyma (Reiley et al., 2010; Sakai et al., 2014). Recently it was also shown that KLRG1-CXCR3+ CD4 T cells circulate in higher numbers in H56/CAF01 immunized mice following infection and that these less differentiated cells have the capacity to readily traffic into the Mtb-infected lung parenchyma (Woodworth et al., 2016). We therefore turned our focus into examining the phenotype of ESAT-6-specific CD4 cells in the lung parenchyma and vasculature following infection/reinfection. In Mtb memory mice, we found that the vast majority (>70%) of ESAT-6-specific CD4 T cells in the lung vasculature were highly differentiated into KLRG1+ cells already 2 weeks into infection. In contrast, a significantly lower proportion of ESAT-6-specific CD4 T cells in the lung vasculature of H56 memory mice expressed KLRG1 during the first 10 weeks of infection (20–40%) (Fig. 4A). Despite these differences, the proportion of KLRG1+ cells progressively increased during later stages in the H56 memory group, so that by week 20 post challenge, both Mtb and H56 mice had equivalent proportions of KLRG1 expressing cells in the lung vasculature (Fig. 4A). Even though KLRG1 expression by ESAT-6-specific CD4 T cells in the lung parenchyma was lower in both sets of mice compared to the vasculature, H56 memory mice also had significantly lower KLRG1 expression in the parenchyma compared to Mtb memory mice during the first 10 weeks of infection (Fig. 4A). Similar to the vasculature compartment, the proportion of KLRG1+ cells in the parenchyma however reached equivalency at 20 weeks post challenge. PD-1 expression was not significantly different

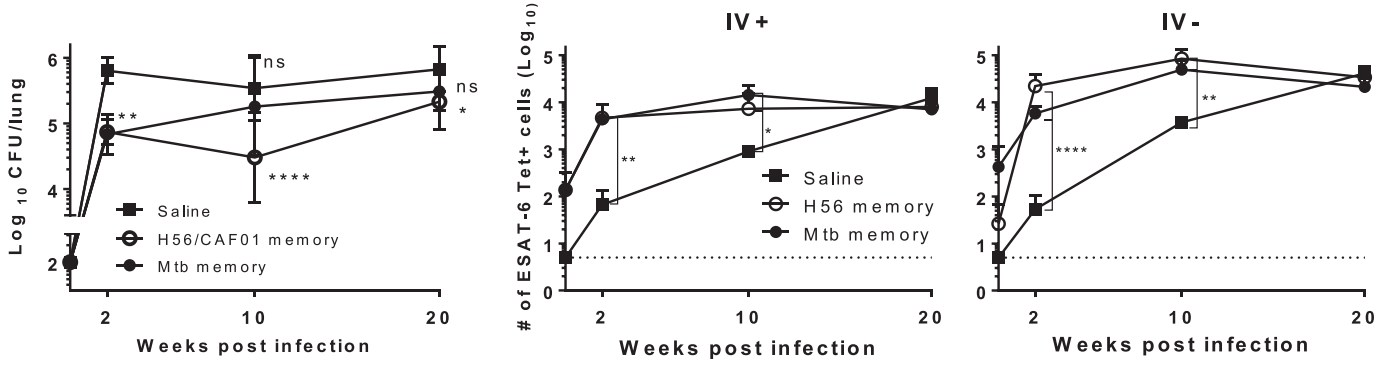

Fig. 2. Mtb memory provides early, but transient, protection to Mycobacterium tuberculosis infection, whereas H56 memory mediates sustained protection accompanied by accelerated recruitment of E6-specific cells into the lung parenchyma. C57BL/6 mice were rested for ~half a year prior to aerosol Mtb challenge (~100 CFU/lung). A) Total lung CFU was determined by serial plating at week 2, 10 and 20 in saline controls (black square), H56 memory (white circle) and Mtb memory (black circle). Data show mean ± s.d. of 8–14 mice/time-point in Saline group, and 6–7 mice/time-point in H56 and Mtb memory – though 4 at week 2 in these two groups. Two way ANOVA with Dunnett's multiple comparison test against Saline group. *$P < 0.05$; **$P < 0.01$, ****$P < 0.0001$. ns non-significant. B) Total number of ESAT-6_{4-17} tetramer binding CD4 T cells within the lung vasculature (IV+) as determined by i.v. staining with anti-CD45 (unperfused lungs). C) Total number of lung parenchymal (IV-) ESAT-6-specific CD4 T cells (unperfused lungs). 3–4 mice/time-point. For B) & C): Cells gated on Singlets > Lymphocytes > Live, non-CD8s ($Dead^-CD8^-$) > $CD3^+CD4^+$ > E6 Tet^+CD44^+. For each time point, One-way ANOVA on log-transformed cell numbers with Tukey's multiple comparison test. *$P < 0.05$; **$P < 0.01$, ****$P < 0.0001$. A repeat experiment with similar overall outcome is shown in Supplementary Fig. 6.

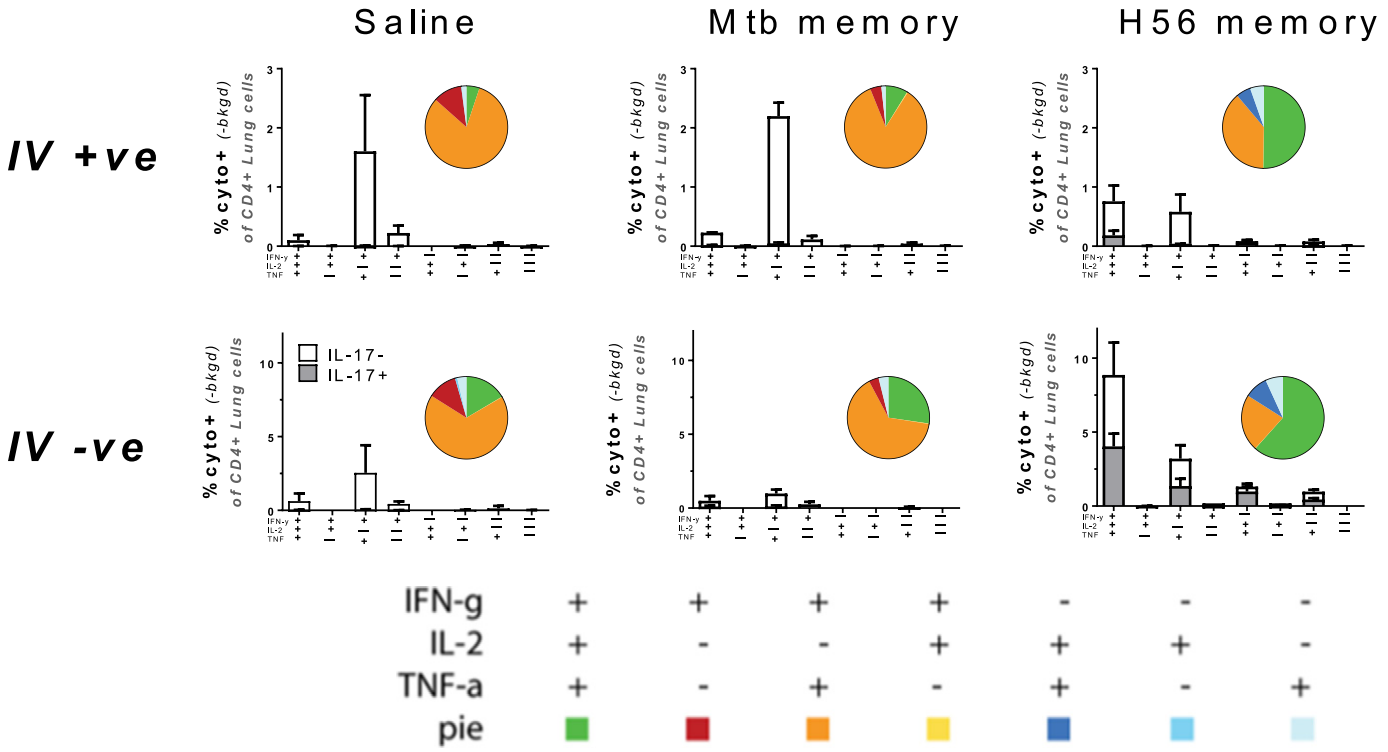

Fig. 3. Secondary effectors among memory mice differ in cytokine multifunctionality with responses in H56 memory mice dominated by IL-2- and IL-17A-producing CD4 T cell subsets. Ten weeks into Mtb challenge, lung cells from memory mice were i.v. stained with anti-CD45 prior to euthanization and subsequently stimulated ex vivo with ESAT-6_{1-15} and stained by ICS to determine the frequency of antigen-specific CD4 T cells expressing IFN-g, TNF-a, IL-2 or IL-17A in any combination based on combinatorial Boolean gating analysis. Upper panels show lung vascular associated responses (IV+); lower panels responses in the lung parenchyma (IV−). Bar charts show mean frequencies ± s.d. ($n = 3$), white bars: IL-17A-; grey bars: IL-17A co-producers. Pies embedded into bar charts denote the proportion of each cytokine-producing subset of the responding cells from each lung compartment (unperfused lungs). Cells gated on Singlets > Lymphocytes > CD4+ > Combinatorial/Boolean gating on IV+, IFN-g+, TNF+, IL-2+, IL-17A+. Repeated once with similar results.

in the lung parenchyma or vasculature of both sets of mice and did not change much within the vasculature. However, its expression showed an equivalent and progressive increase in the parenchyma up to 20 weeks post challenge (Fig. 4B). A large proportion of ESAT-6 specific iv+ cells expressed ICOS early during infection especially in the H56 memory mice, but this proportion dropped from week 2 onwards in both groups (Fig. 4C). Like PD-1, ICOS expression was more pronounced among lung parenchyma ESAT-6-specific CD4 T cells and the respective proportions of ICOS expressing cells was not different between H56 and Mtb memory in the lung parenchyma (Fig. 4C). Thus, based on KLRG1 expression levels, secondary ESAT-6-specific effectors in Mtb mice were rapidly driven into a higher differentiation state not only in the lung vasculature, but even within the parenchyma, which is otherwise dominated by KLRG1 − subsets. Of note, a high proportion of KLRG1 + cells was observed in Mtb memory mice at week 2, thus preceding the loss of protection in this group. Similarly, the increase in the proportion of KLRG1 + cells seen in late stage infection of H56 memory mice temporarily occurred coincident with the narrowing of the protective window in these memory mice.

Antigen availability is a key factor responsible for driving increased differentiation, both during priming of Mtb memory responses, but also for pushing already fully differentiated CD4 T cells into terminal differentiation during subsequent challenge (Moguche et al., 2017). We therefore compared KLRG1 expression on lung parenchyma ESAT-6- and Ag85B-specific CD4 T cells. ESAT-6 and Ag85B are distinct Mtb antigens that differ in their expression pattern during infection with ESAT-6 being expressed and recognized continuously by cognate cells throughout infection, in contrast to Ag85B that is highly expressed early in the infection but not late (Hoang et al., 2013; Kremer et al., 2002; Moguche et al., 2015; Moguche et al., 2017; Rogerson et al., 2006; Shi et al., 2004). Ten weeks post challenge; we found that the proportion of ESAT-6-specific CD4 T cells in the lung parenchyma expressing KLRG1 was significantly higher than for Ag85B-specific CD4 T cells in Mtb memory mice ($P < 0.01$; Fig. 5A). Indeed, even on a per cell basis, ESAT-6-specific CD4 T cells expressed more KLRG1 than their Ag85B counterparts ($P < 0.001$; Fig. 5B). Although at a much smaller scale, a similar trend was also seen between ESAT-6- and Ag85B-specific CD4 T cells in the lung parenchyma populations of H56 memory mice at 10 weeks post challenge (Fig. 5). Additionally, KLRG1 expression as a proportion of cells and on a per cell basis; was higher for Mtb-specific CD4 T cells from Mtb memory mice compared to H56 memory mice (Fig. 5). This was highly significant for ESAT-6-specific cells, but on a per cell basis also seen among Ag85B-specific CD4 T cells in Mtb memory compared to H56 memory mice ($P < 0.05$, Fig. 5B). Taken together, this data suggests that the nature of T cells priming (mycobacterial infection vs. subunit vaccination) impacts the differentiation status of T cell memory.

3.5. H56/CAF01 Induced Memory Cells Home to the Lung Parenchyma More Efficiently Compared to Memory Cells Generated After Mycobacterial Infections

As ESAT-6-specific memory T cells in Mtb memory mice were more differentiated than those in H56/CAF01 vaccinated mice and seemed to be less efficiently recruited to the lung after Mtb infection, we hypothesized that Mtb- and H56-primed memory cells differ in their inherent capacity to home to the infected lung parenchyma. To formally test this hypothesis, we undertook adoptive transfer experiments, where long-term Mtb and H56 memory CD4 T cells were co-adoptively transferred into the same chronically infected hosts. Although purified CD4 T cells were transferred at the equivalence of 1 to 1 Mtb:H56 memory mice per recipient (a 1:1 ratio), subsequent analysis of the pooled donor cells revealed that these consisted of 63% from H56 memory and 37% from Mtb memory mice, thus corresponding to a 1.7: 1 ratio

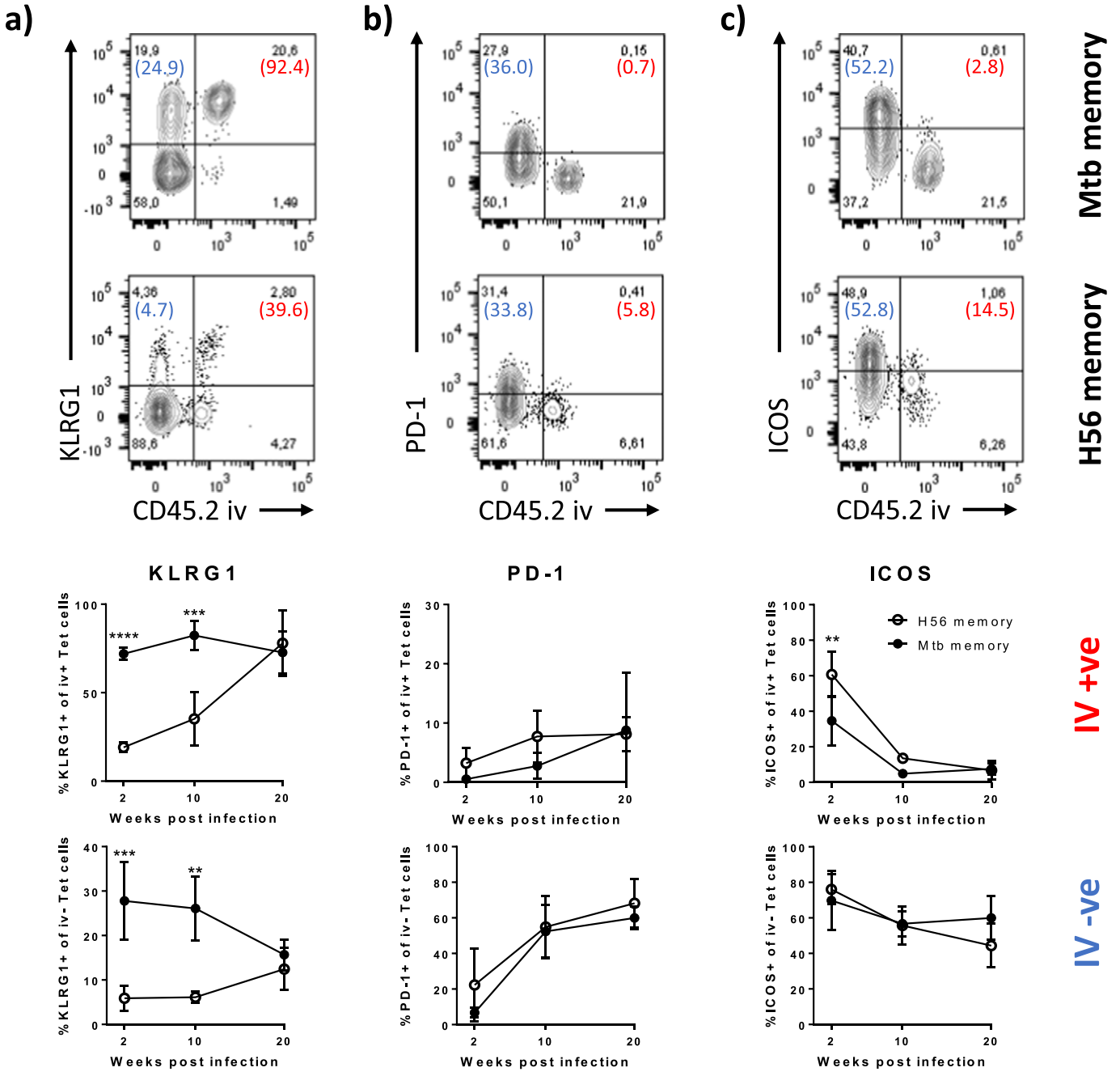

Fig. 4. ESAT-6-specific effectors in Mtb memory mice exhibit increased differentiation within the lung parenchyma early during infection compared to H56 memory mice. A) KLRG1 expression among lung localized I-A^b:ESAT-6-specific CD4 T cells. Representative FACS plots showing KLRG1 expression on ESAT-6$_{4-17}$ tet+ cells from Mtb (upper plot) and H56 (lower plot) memory mice infected for ten weeks with *Mycobacterium tuberculosis* relative to their localization in the lung vasculature (CD45.2 IV +ve) or lung parenchyma (CD45.2 IV –ve). Numbers in parentheses represent the percentage of cells expressing KLRG1 in the IV +ve (Red) and the IV −ve population (Blue). Graphs show the proportion of KLRG1+ of I-A^b:ESAT-6$_{4-17}$ tetramer+ CD4 T cells in the lung vasculature (IV +ve; upper graph) and in the lung parenchyma (IV –ve, lower graph) over the course of infection (unperfused lungs). Mean ± s.d. of 3–4 mice per group at any given time-point. Two-way ANOVA with Sidak's multiple comparison test for simple row effects. Differences between Mtb and H56 memory. $^{****}P < 0.0001$, $^{***}P < 0.001$, $^{**}P < 0.01$. B) PD-1 expression among lung localized I-A^b:ESAT-6-specific CD4 T cells. Representative FACS plots showing PD-1 expression on ESAT-6$_{4-17}$ tet+ cells from Mtb (upper plot) and H56 (lower plot) memory mice infected for ten weeks with *Mycobacterium tuberculosis* relative to their localization in the lung vasculature (CD45.2 IV +ve) or lung parenchyma (CD45.2 IV –ve). Numbers in parentheses represent the percentage of cells expressing PD-1 in the IV +ve (Red) and the IV −ve population (Blue). Graphs show the proportion of PD-1+ of I-A^b:ESAT-6$_{4-17}$ tetramer+ CD4 T cells in the lung vasculature (IV +ve; upper graph) and in the lung parenchyma (IV –ve, lower graph) over the course of infection (unperfused lungs). Mean ± s.d. of 3–4 mice per group at any given time-point. Two-way ANOVA with Sidak's multiple comparison test for simple row effects (ns). C) ICOS expression among lung localized I-A^b:ESAT-6-specific CD4 T cells. Representative FACS plots showing ICOS expression on ESAT-6$_{4-17}$ tet+ cells from Mtb (upper plot) and H56 (lower plot) memory mice infected for ten weeks with *Mycobacterium tuberculosis* relative to their localization in the lung vasculature (CD45.2 IV +ve) or lung parenchyma (CD45.2 IV –ve). Numbers in parentheses represent the percentage of cells expressing ICOS in the IV +ve (Red) and the IV –ve population (Blue). Graphs show the proportion of ICOS+ of I-A^b:ESAT-6$_{4-17}$ tetramer+ CD4 T cells in the lung vasculature (IV +ve; upper graph) and in the lung parenchyma (IV –ve, lower graph) over the course of infection (unperfused lungs). Mean ± s.d. of 3–4 mice per group at any given time-point. Two-way ANOVA with Sidak's multiple comparison test for simple row effects. Differences between Mtb and H56 memory. $^{**}P < 0.01$. Gating as depicted in Supplementary Fig. 4. One of two comparable experiments shown.

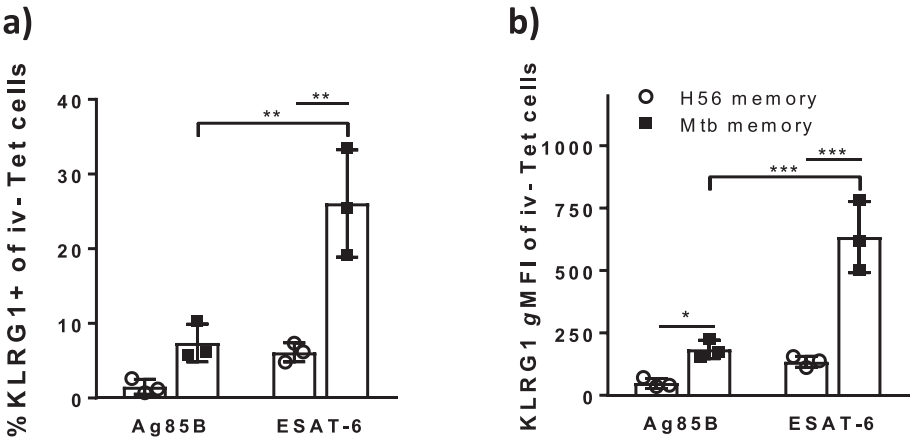

Fig. 5. ESAT-6 specific secondary effectors express significantly more KLRG1 than Ag85B-specific CD4 T cells in Mtb memory mice in contrast to H56 memory mice. Ten weeks into infection of rested C57BL/6 memory mice, the frequency of KLRG1+ cells and the expression levels of KLRG1 within the lung parenchyma (IV –ve population) was assessed after i.v. injection of anti-CD45.2-FITC prior to tissue harvest (unperfused lungs) using I-A^b:$Ag85B_{280–294}$ and I-A^b:ESAT-$6_{4–17}$ specific tetramer staining. A) Bar chart showing the frequency of $Ag85B_{280–294}$ and ESAT-$6_{4–17}$ specific CD4 T cells being KLRG1+ within the IV –ve lung population ten weeks into challenge of H56 (white) and Mtb memory (black) mice. Two-way ANOVA with Tukey's multiple comparison test. $^{**}P < 0.01$. B) Bar chart showing the KLRG1 gMFIs of $Ag85B_{280–294}$ and ESAT-$6_{4–17}$ specific CD4 T cells within the lung parenchyma (IV –ve) ten weeks into challenge of H56 (white) and Mtb memory (black) mice. Two-way ANOVA with Tukey's multiple comparison test. $^{***}P < 0.001$, $^{*}P < 0.05$. Gating as depicted in Supplementary Fig. 4. The experiment was repeated once with similar results.

of E6-specific CD4 T cells from H56 vs Mtb memory mice (Supplementary Fig. 5A). Based on ESAT-$6_{4–17}$:I-A^b tetramer pulldown and intravascular labeling of the recipients, the proportion of donor H56 memory ESAT-6-specific cells that had migrated into the lung parenchyma (iv−) was found significantly higher than that of donor Mtb memory cells (Fig. 6A&B, Supplementary Fig. 5). These results indicated an inherent inferior ability of Mtb memory CD4 T cells to migrate into the lung parenchyma. We next speculated whether the limitation of the Mtb memory T cells was related to the presentation of the antigens to the immune system in the context of a live and replicating mycobacteria vs. H56 vaccination, where ESAT-6 and Ag85B antigens are presented in a non-replicating form. As BCG vaccination employs a live attenuated *M. bovis* strain sharing several characteristics with the real Mtb, we compared the BCG vaccine induced memory CD4 T cells to those of H56/CAF01. We immunized congenically marked mice either with a single dose of BCG, or with three weekly doses of H56/CAF01. As BCG does not contain ESAT-6, we focused on Ag85B for analysis of antigen-specific CD4 T cells. Mice were analyzed at two months post vaccination (for H56/CAF01 this was after the last dose). Both BCG and H56 vaccination induced a population of memory Ag85B-specific CD4 T cells in the lymphoid tissues (spleen and lymph nodes) (Fig. 6C). Just as in Mtb memory, BCG vaccination induced more expression of KLRG1 compared to H56/CAF01 that hardly induced any KLRG1 expression. Additionally, H56/CAF01 memory cells had a higher expression of PD-1 compared to BCG memory cells (Fig. 6C), a situation reminiscent of Mtb memory (Fig. 1C & Supplementary Fig. 2). Thus BCG vaccination, just like Mtb, drove memory CD4 T cells to a more differentiated stated compared to H56 vaccination. This trait was also recapitulated when comparing BCG-driven CD4 T cell responses against TB10.$4_{74–88}$ to responses after an Mtb infection partially cleared by 6 weeks of INH/RIF treatment in CB6F1 mice (Supplementary Fig. 3). To address the impact on migration and lung homing, we co-transferred H56 and BCG memory cells intravenously into chronically infected, congenically marked host mice. At 18–20 hour post transfer, we assessed their migration into the lung parenchyma using the intravascular labeling technique and $Ag85B_{280–294}$:I-A^b tetramers. Similar to Mtb memory cells, we found that BCG memory CD4 T cells had an inferior capacity to migrate into the lung parenchyma compared to H56 memory cells (Fig. 6D). Collectively, these findings show that both Mtb and BCG primed memory cells are impaired in their ability to migrate into the infected lung parenchyma and suggest an inherent trait of memory responses promoted by their nature of initial priming.

4. Discussion

A significant proportion of TB patients successfully cured after chemotherapy exhibit recurrent disease. Similar to recrudescence of a latent infection, many of these cases can be ascribed to reactivation of residual bacilli after treatment failure but, especially in high-incidence areas, exogenous re-infections seem to account for a significant proportion of TB recurrence (De Boer & Van Soolingen, 2000; Guerra-Assuncao et al., 2015; Sonnenberg et al., 2001; Uys et al., 2015; Verver et al., 2005). Such TB patients could simply just be inherently more susceptible, thus exhibiting recurrent infections. However, these observations might also suggest that memory responses after natural exposure provide insufficient protection against recrudescent infection(s) or reinfection(s) with Mtb – either due to lack of T cell epitope reactivity (Scriba et al., 2017) or due to the nature of response. Here we show that ESAT-6 specific CD4 memory T cells generated after an Mtb infection cleared by treatment are fully differentiated along the Th1 axis, and that their protective capacity is inferior to memory cells induced by H56/CAF01 subunit vaccination, which show a lower degree of differentiation. These differences in differentiation state were maintained both in long-term resting memory cells as well as in secondary responses. We thus posit that the degree of differentiation and qualitative responses thereafter are dictated by the nature of initial priming and that live mycobacteria induce inherently inferior memory T cells.

In the present study we confirm earlier observations that less differentiated T cells have an increased ability to migrate into the parenchyma. First, we show that less differentiated ESAT-$6_{4–17}$ specific CD4 memory T cells primed by H56/CAF01 vaccination have accelerated recruitment into the lung parenchyma compared to more differentiated memory cells primed by natural infection. This observation is consistent with our recent report demonstrating accelerated parenchymal recruitment of secondary effectors after H56/CAF01 vaccination (Woodworth et al., 2016). Secondly, using a co-adoptive transfer approach, we directly demonstrate that less differentiated Mtb-specific CD4 memory T cells primed by H56/CAF01 have a selective and significantly enhanced capacity to home to the infected lung parenchyma compared to mycobacteria-primed T cells of a higher differentiation state. The lower recovery of Mtb memory donor cells from the lung compartments of the recipients (relative to the transferred 1.7:1 ratio of ESAT-6 specific H56 memory vs Mtb donor cells) suggests that some of the transferred Mtb memory cells did not reach the lungs and might have homed to sites of disseminated infection. The fact that the majority of ESAT-6

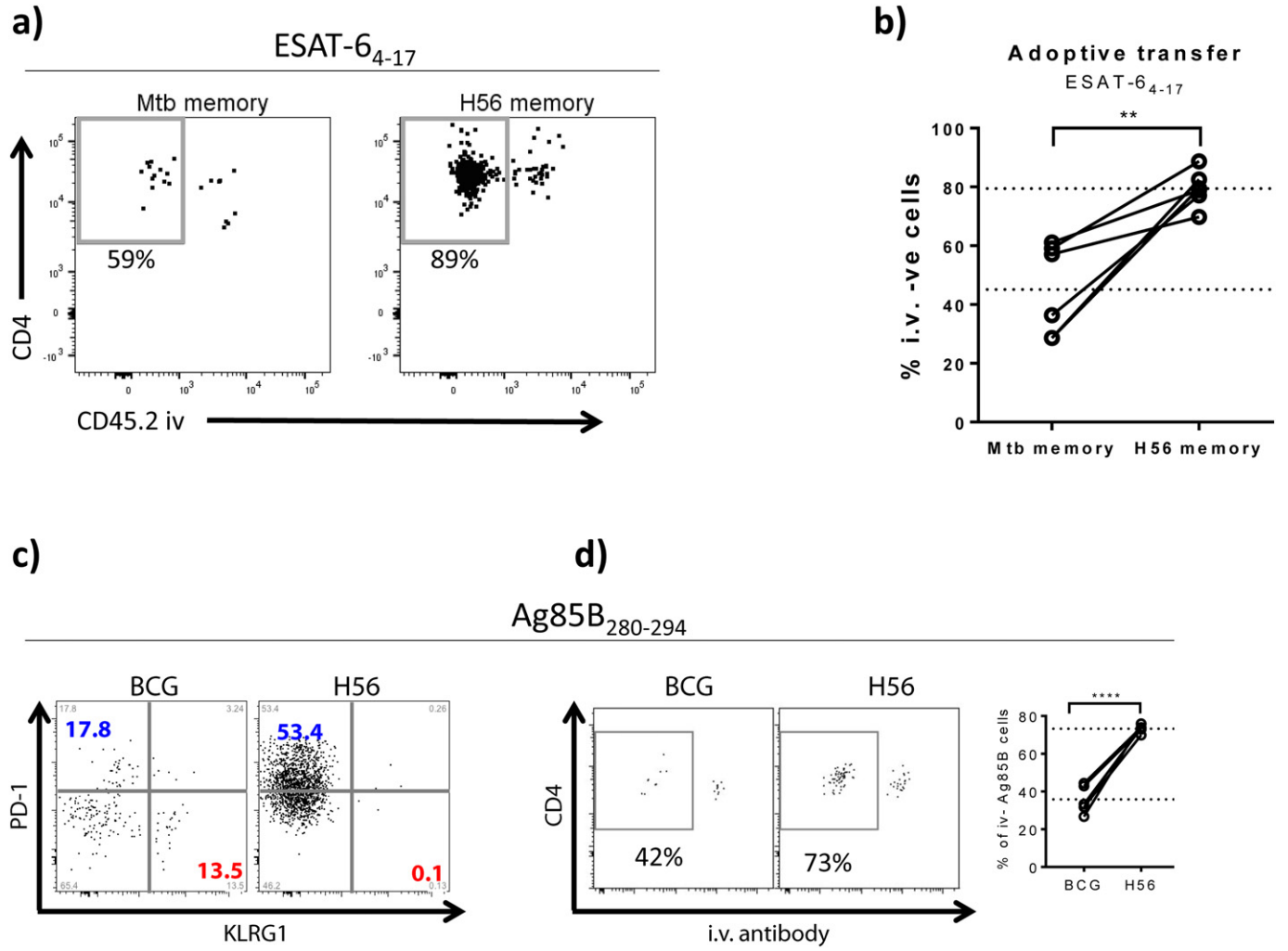

Fig. 6. Antigen-specific CD4 T cells primed by mycobacteria are less efficient at migrating into the infected lung parenchyma than cells primed by H56/CAF01 vaccination in co-adoptive transfer experiments. A) CD4 T cells from long term H56 and Mtb memory mice were isolated from spleens and draining lymph nodes (inguinal and tracheobronchial, respectively) by negative selection and differentially stained with CPD450 (H56 memory) and CPD670 (Mtb memory) cell trackers, admixed in a ~1:1 ratio and adoptively transferred into recipient mice chronically infected with Mtb for 34 weeks. Location of I-A^b:ESAT-6_{4-17}-specific cells from each donor origin was assessed 16–18 h post transfer using tetramer-specific pulldown following i.v. administration of anti-CD45 just prior to euthanasia (unperfused lungs). Representative FACS plots showing ESAT-6 specific lung cells after enrichment using I-A^b:ESAT-6_{4-17}-specific tetramer pulldown. The two plots show the distribution in the lung compartment of ESAT-6_{4-17} specific cells originating from Mtb memory donors (left) and H56 memory donors (right). The gate shows the percentage of ESAT-6_{4-17} specific cells of Mtb memory vs H56 memory origin within the infected lung parenchyma (iv –ve). Gating as depicted in Supplementary Fig. 5. B) Graph showing the percentage of ESAT-6_{4-17} specific cells of Mtb memory vs H56 memory donor origin within the I.V. –ve compartment (parenchyma) when co-adoptively transferred into the same infected recipients. Dotted lines depict mean values. Student's *t*-test, paired $^{**}P < 0.01$. C) Congenic C57BL/6 mice were immunized with either 1× BCG (CD45.1) or 3× H56/CAF01 (CD45.2) and CD4 T cells purified by negative selection at ~50 days post vaccination. BCG and H56 memory cells were mixed in a1:1 ratio and Ag85B-sepcific responses characterized by I-A^b: $Ag85B_{280–294}$ tetramer staining. $Ag85B_{280–294}$ specific H56 (CD45.2) and BCG (CD45.1) memory cells were phenotypically characterized in terms of PD-1 and KLRG1 expression. No KLRG1 expressing Ag85B-specific cells were detected among H56 memory cells (left plot), which were dominated by PD-1 expression (blue). In contrast, a notable proportion of $Ag85B_{280–294}$-specific cells primed by BCG (right plot) was found to express KLRG1 (red). D) Memory cells from BCG (CD45.1) and H56 (CD45.2) vaccinated mice were co-adoptively transferred into congenically-mismatched recipients carrying a 10 week old Mtb infection. Location of I-A^b: $Ag85B_{280–294}$-specific cells from each donor origin was assessed based on their congenic markers (CD45.1 vs CD45.2) 20 h post transfer using tetramer-specific pulldown assays after i.v. labeling. Representative FACS plots showing the distribution of $Ag85B_{280–294}$-specific memory cells primed by either BCG or H56/CAF01 within the lung of infected recipient mice. Graph summarizes the percentage of $Ag85B_{280–294}$-specific memory cells primed by either BCG or H56/CAF01 within the parenchyma (I.V. – compartment) after co-adoptive transfer into the same recipients. Dotted lines depict mean values. Student's *t*-test, $^{****}P < 0.0001$. C & D – one representative experiment out of three repeat experiments shown.

memory cells in both Mtb and H56 memory mice were found to be CXCR3 +, suggests that CXCR3 is probably not the main receptor that govern homing to the lung following Mtb infection (Moguche et al., 2015; Sakai et al., 2014). This advocates for a certain degree of redundancy among chemokine receptors, integrins and adhesion molecules that control entry to the Mtb infected lung parenchyma (Behar et al., 2014; Ghosh et al., 2006). Factors that control retention and intra-lesional positioning of T cells within the infected lung parenchyma would however be of equally high importance. Thus, although CD69 and CD103 is primarily known to promote tissue retention under homeostatic conditions (Sheridan & Lefrancois, 2011), they cannot be precluded to play a similar role for lung tissue retention in the inflammatory settings of a Mtb infection (Sallin et al., 2017). Likewise, the α1 integrin (CD49a) has been shown to stabilize Mtb granulomas and could therefore play a role for positioning T cells once in the lung parenchyma (Taylor et al., 2008). In preliminary work, we have found several of these markers useful for delineating iv + and iv − subsets, and future work aim to identify and understand the factors involved in lung parenchymal retention and intra-lesional migration of vaccine-promoted memory cells.

Similar to most mouse studies on the protection against post-primary Mtb infection (Cooper et al., 1997; Henao-Tamayo et al., 2012; Jung et al., 2005; Kamath & Behar, 2005; Mollenkopf et al., 2004), we found that Mtb memory mice were significantly protected,

but that this protection was lost during later stages of infection. In earlier studies using a similar Mtb memory model, Henao-Tamayo et al. (Henao-Tamayo et al., 2012) showed that natural memory only provided short-term protection to reinfection, when memory mice were challenged shortly after sterilizing chemotherapy. In the current study, where Mtb memory responses were allowed to reach a quiescent, and potentially more protective, state, protection was still short-lived. Hence, whereas H56 memory mediated sustained protection until week 20, Mtb memory mice were only transiently protected, and no significant protection could be detected from week 10 and onwards. Even though H56 memory mice had a superior and longer protective window compared to Mtb memory, this window also progressively narrowed. Prior studies in the Mtb memory model have shown that while the transient period of protection provided was associated with smaller lymphocytic lesions, the loss of protection was accompanied by a concomitant and copious increase in lung damage with extensive foci of inflammation and consolidation (Henao-Tamayo et al., 2012). In the C57BL/6 or CB6F1 mice, lung histopathology generally correlates closely with bacterial burden (Dietrich et al., 2015), and subunit vaccines that mediate significant reductions in lung bacterial burden do also protect against progressive pulmonary pathology (Baldwin et al., 2016; Counoupas et al., 2017). In line with this, we have previously shown that CAF01-adjuvanted preventive vaccination in mice leads to a decrease in neutrophil accumulation and pathology in the lung over non-vaccinated controls (Woodworth et al., 2014), and H56/CAF01 immunization additionally reduces lung pathology in terms of number of lesions and lesion size when administered during post-exposure settings (Aagaard et al., 2011) & Billeskov et al. submitted. In terms of histopathology, the mouse models possess certain limitations, as Mtb lesions differ from human lung pathology. Importantly, H56 administered in either CAF01 or IC31 as a BCG booster reduced pulmonary pathology and extrapulmonary dissemination in cynomolgus macaques (Billeskov et al., 2016; Lin et al., 2012), where lung pathology closely resembles the histopathological manifestations in man. Likewise, immunization with earlier H-series vaccines have shown to reduce pathology scores in lungs and other organs in NHP models (Billeskov et al., 2013; Langermans et al., 2005).

Sustained protection against Mtb has previously been linked to a continuous recruitment of less differentiated KLRG1- CD4 T cells with the capacity to produce IL-2 (Lindenstrøm et al., 2013). Woodworth et al. (Woodworth et al., 2016) recently showed that KLRG1 − CXCR3 + CD4 T cells within the peripheral circulation and lung vasculature represent newly lymphoid emigrants capable of entering the Mtb infected lung parenchyma. A continuous migration of such KLRG1 − CXCR3 + cells from the lymph nodes to the lung parenchyma could be a key underlying feature for sustained protection. In our study, we find that highly differentiated KLRG1 + cells dominated the ESAT-6 specific CD4 T cell pool in the lung vasculature of Mtb memory immune animals already early during infection. This could potentially compromise long-term protection due to limited recruitment of less differentiated cells and thus less replacement of terminally differentiated cells within the lung parenchyma. We speculate that a continuous influx of KLRG1 − cells could renew the parenchymal T cell population, limit progression to terminal differentiation and thereby prevent terminal exhaustion. The notable increase in iv + KLRG1 + ESAT-6 specific CD4 T cells in H56 memory mice from week 10 to 20 post infection concomitant with a narrowing of the protective window would be in thread with this interpretation. In addition, significantly more ESAT-6 specific T cells were KLRG1 − among the iv + cell pool during the first 10 weeks of infection in H56 memory mice compared to Mtb memory immune mice, where protection failed. Interestingly, the dominance of less differentiated secondary effectors in the lung vasculature of H56 memory mice was directly mirrored by their increased capacity to produce IL-2, consistent with findings that KLRG1 −/less differentiated CD4 T cells are the main producers of IL-2 (Torrado et al., 2015; Woodworth et al., 2016). IL-2 producing CD4 T cell subsets were generally more frequent among the less differentiated parenchymal cells and again found to be much more dominant in the H56 memory mice. Terminal differentiation of the parenchymal CD4 T cells in Mtb memory mice was reflected by the fact that much fewer cells produced Th1 cytokines (incl. IFN-γ) in response to ESAT-6_{1-15} stimulation, suggestive of partial exhaustion, which might have contributed to the lack of containment. On a phenotypic level, the early loss of protection seen in Mtb memory mice was associated to high differentiation of primarily ESAT-6-specific, but also to some extent Ag85B-specific, cells within the parenchyma. This was manifested as significantly increased levels of KLRG1 expression, both in terms of the proportion of parenchymal cells as well as on a single cell level as compared to H56 memory mice. Our studies therefore suggest that differences in addition to parenchymal trafficking and quantity play a significant role, which may overcome trafficking and quantitative advantages. For instance, Mtb memory mice had significantly more ESAT-6 specific cells in the parenchyma than naïve mice at week 10 – yet these cells did not mediate protection. In addition, both Mtb and H56 memory had equivalent total numbers of ESAT-6-specific CD4 T cells in the lung parenchyma 10 weeks post challenge, yet H56 memory mice harbored ~5 times less bacteria compared to Mtb memory mice. Indeed, the significance of this finding is striking since at 2 weeks post infection, both groups had the same level of protection, despite Mtb memory mice started with more memory cells (though ns) in the lung parenchyma than H56 memory mice. Part of the explanation is likely due to the accelerated migration by H56 memory cells, leading to equivalency by week 2. However, this also underscore that qualitative differences in parenchymal T cells (e.g. cytokine production, parenchymal retention and positioning), might be similar or even more critical than the per se migration into the parenchyma. This would be in line with very recent data from Rhesus macaques, showing that in this model of non-chronic TB, positioning of CXCR3 + CXCR1-PD-1^{hi}CTLA + parenchymal CD4 T cells relative to granulomatous lesions play a more important role than the actual extravasation to the parenchyma (Kauffman et al., 2017).

ESAT-6 specific CD4 T cells in the lungs of Mtb infected mice exhibited extensive contraction within the first 6 weeks of INH/RIF treatment. This is in accordance with the notion that KLRG1 + T cells are not self-renewing (Reiley et al., 2010) and undergo extensive attrition shortly after transfer into uninfected hosts (Moguche et al., 2015). At first sight, the sustainment of KLRG1 + cells at week 40, long after EoT, seems at odds with a T cell population that requires antigen for its survival. This suggests that treated Mtb memory mice harbor remaining antigen derived either from dead bacteria or from dormant/uncultivable bacteria. Such non-resolved antigen could sustain the survival of KLRG1 + CD4 T cells, but potentially also render memory formation dysfunctional in the Mtb memory mice. In contrast, PD-1 + memory cells are known to survive in the absence of antigenic stimulation, but require ICOS-ICOSL interactions for their survival (Moguche et al., 2015). However, although most H56 memory cells expressed PD-1 and ICOS during the first several weeks after priming, most H56 memory cells had lost expression of these markers at week 40. In accordance, although Mtb-primed CD4 T cells were sustained after transfer into uninfected wt mice, most cells lost PD-1 expression within 4 weeks (Moguche et al., 2015). Hence, PD-1 expression on memory cells might not be stably expressed during quiescent, homeostatic conditions. In line with this, signaling through the ICOS-ICOSL axis was essential for memory formation, but dispensable for survival of, CD4 T_{CMs} in a *Listeria monocytogenes* infection model (Marriott et al., 2015).

T cell priming critically depends on antigen affinity, dose and duration, which are all known to impact the imprint and differentiation state of the ensuing memory responses (Blair et al., 2011; Keck et al., 2014). Continuous (e.g. Mtb infection), or protracted (as presented by BCG), antigen exposure is thus a central factor for driving terminal differentiation of Mtb-specific CD4 T cells. For instance Ag85B, expressed at low levels during chronic Mtb infection, renders Ag85B-specific CD4 T cells less terminally differentiated than ESAT-6-specific CD4 T cells

(e.g. Fig. 5) (Moguche et al., 2017), whereas infection using a recombinant Mtb with forced constitutive expression of Ag85B has been shown to drive Ag85B specific cells to terminal differentiation at levels similar to their ESAT-6 counterparts (Moguche et al., 2017). Antigen dose during vaccination not only affects the magnitude of CD4 T cell responses (Aagaard et al., 2009), but also their differentiation state, with higher doses leading to increased function differentiation of CD4 T cells in QTF + ve individuals (Moguche et al., 2017). Likewise, increasing the H56 dose in preventive immunization of mice leads to priming of CD4 T cells with higher KLRG1 expression (J. Woodworth Unpublished, Pers. Comm.). In addition to Ag-availability, factors such as TCR affinity (Baumgartner et al., 2012), co-stimulatory receptors (Kawalekar et al., 2016) as well as the cytokines present during priming (Au-Yeung et al., 2017; Schluns & Lefrancois, 2003) all play a distinct role for imprinting T cells of a given differentiation state. Hence, T cell differentiation state is in part controlled by graded T-bet expression, which to a large extent is dictated by the nature of inflammation during the priming process (Joshi et al., 2007). In preliminary studies, we find that increasing the inflammatory potential of CAF01 by addition of Poly I:C and CpG, leads to priming of CD4 T cells with higher KLRG1 expression (unpublished data). ESAT-6 specific CD4 T cells in mice with IL-27RA deficiency was in contrast shown to exhibit lower T-bet expression and less transition into KLRG1 + subsets after Mtb infection and similarly, T-bet haploinsufficiency prevented the differentiation to KLRG1 + subsets (Torrado et al., 2015). Furthermore, downstream signaling through the IL-12/23p40 axis was recently shown to regulate T-bet expression in primed T cells, and influenced both terminal differentiation and lung localization during Mtb infection (Sallin et al., 2017). Live Mtb and BCG could additionally be expected to be taken up by different DC subsets compared to subunit vaccines administered by the s.c. route leading to priming of T cells that differ in chemokine receptor expression patterns and thus tissue homing properties. Whereas DC subsets and tissue tropic signals such as retinoic acid and vitamin D3 has been identified for the imprint of gut and skin homing T cells subsets respectively, less is however known regarding the signals that imprint T cells with tropism for the lung (Baaten et al., 2013). The integration of all these signal during primary T cell activation determines unique and long lasting T cell differentiation programs that are maintained during recall responses (Keck et al., 2014). Through epigenetic regulations, activated, poised vs repressed gene expression patterns are retained in the descendants of such memory cells, and the phenotype of secondary effectors may therefore to some extent be defined already during the initial priming (Weng et al., 2012).

CAF01–adjuvanted subunit vaccines induce a diverse range of T helper cells including bona fide Th1 cells (T-bet$^+$CXCR3$^+$), Th17 (Ror-γt$^+$) and T_{FH} (CXCR5$^+$PD-1$^+$Bcl-6$^+$) as well as T helper cells that co-express multiple T-cell lineage-specifying transcription factors (Prota et al., 2015) (& not published). CAF01 primed CD4 memory T cells are characterized by a large capacity for IL-2 and IL-17 production (Knudsen et al., 2016; Lindenstrøm et al., 2009; Lindenstrøm et al., 2012), and share a number of features with T_{FH}-like cells. Such T_{FH}-like properties have been linked to improved Th1 maintenance and protection against Mtb challenge (Moguche et al., 2015) as well as to the generation of long-lived T_{CM} (Pepper et al., 2011). BCG and Mtb infection share a number of features in T cell priming, including sustained Ag-availability and inflammatory signaling that ultimately leads to induction of fully differentiated Th1 cells with high T-bet expression. Similar to earlier reports (Lindenstrøm et al., 2009; Nandakumar et al., 2014), we found that BCG imprints vaccine responses with several features of the response driven by the real Mtb infection. Hence, BCG promoted Ag85B-specific CD4 T cells were more differentiated along the Th1 axis compared to H56/CAF01 immunization. Analogous to the Mtb-driven ESAT-6 memory responses, BCG promoted Ag85B specific cells were significantly impaired in migrating into the Mtb infected lung parenchyma in co-adoptive transfer experiments with Ag85B specific cells primed by H56/CAF01. Ultimately this suggests that CD4 memory T cells primed by mycobacteria could be inherently impaired due to their high differentiation state, not only in terms of their lung migratory capacity, but also qualitatively once in the parenchyma. This needs to be accounted for in the development of novel vaccines to ensure priming of memory responses capable of generating secondary effectors with a strong lung homing capacity that can mediate durable protection against infection with *Mycobacterium tuberculosis*.

Acknowledgement

We acknowledge the NIH Tetramer Core Facility for provision of I-A^b:ESAT-6_{4-17}, I-A^b:Ag85B$_{280-294}$, I-A^d:TB10.4_{70-84}-and corresponding negative control tetramers I-A^b:hCLIP/I-A^d:hCLIP. Linda Christensen is thanked for her excellent technical help. The animal technicians and veterinarians at the Statens Serum Institut are likewise gratefully acknowledged for their excellent assistance. Finally, Joshua Woodworth is thanked for several fruitful discussions on data pertaining to this work.

Funding Sources

This work was supported by the European Commission through the TBVAC2020 consortium contract H2020-PHC-2014-2015-643381 and through the ADITEC consortium (Grant agreement #280873). Funding sources had no role in writing the manuscript or in the decision to submit for publication.

Conflict of Interest

P.A. is co-inventor of patents covering the use of CAF01 as an adjuvant as well as patents relating to tuberculosis fusion protein H56 (Ag85B-ESAT-6-Rv2660c). The authors have no other relevant affiliations or financial involvement with any organization or entity with a financial interest in or financial conflict with the subject matter or materials discussed in the manuscript apart from those disclosed.

Author Contributions

Conceived the idea: TL, EMA, KU, PA. Designed experiments: TL, AM. Performed the experiments: TL, MD, AM. Analyzed data: TL, AM. Writing – original draft: TL, PA. Writing – editing, reviewing, proofreading: TL, PA, AM, KU, EMA, MD.

Appendix A. Supplementary data

Supplementary data to this article can be found online at https://doi.org/10.1016/j.ebiom.2017.12.004.

References

Aagaard, C., Hoang, T.T., Izzo, A., Billeskov, R., Troudt, J., Arnett, K., Keyser, A., Elvang, T., Andersen, P., Dietrich, J., 2009. Protection and polyfunctional T cells induced by Ag85B-TB10.4/IC31 against *Mycobacterium tuberculosis* is highly dependent on the antigen dose. PLoS One 4:e5930. https://doi.org/10.1371/journal.pone.0005930.

Aagaard, C., Hoang, T., Dietrich, J., Cardona, P.J., Izzo, A., Dolganov, G., Schoolnik, G.K., Cassidy, J.P., Billeskov, R., Andersen, P., 2011. A multistage tuberculosis vaccine that confers efficient protection before and after exposure. Nat. Med. 17:189–U224. https://doi.org/10.1038/nm.2285.

Andersen, P., Smedegaard, B., 2000. CD4$^+$ T-cell subsets that mediate immunological memory to *Mycobacterium tuberculosis* infection in mice. Infect. Immun. 68, 621–629.

Au-Yeung, B.B., Smith, G.A., Mueller, J.L., Heyn, C.S., Jaszczak, R.G., Weiss, A., Zikherman, J., 2017. IL-2 modulates the TCR signaling threshold for CD8 but not CD4 T cell proliferation on a single-cell level. J. Immunol. 198:2445–2456. https://doi.org/10.4049/jimmunol.1601453.

Baaten, B.J., Cooper, A.M., Swain, S.L., Bradley, L.M., 2013. Location, location, location: the impact of migratory heterogeneity on T cell function. Front. Immunol. 4:311. https://doi.org/10.3389/fimmu.2013.00311.

Baldwin, S.L., Reese, V.A., Huang, P.W., Beebe, E.A., Podell, B.K., Reed, S.G., Coler, R.N., 2016. Protection and long-lived immunity induced by the ID93/GLA-SE vaccine candidate

against a clinical *Mycobacterium tuberculosis* isolate. Clin. Vaccine Immunol. 23: 137–147. https://doi.org/10.1128/CVI.00458-15.
Baumgartner, C.K., Yagita, H., Malherbe, L.P., 2012. A TCR affinity threshold regulates memory CD4 T cell differentiation following vaccination. J. Immunol. 189: 2309–2317. https://doi.org/10.4049/jimmunol.1200453.
Behar, S.M., Carpenter, S.M., Booty, M.G., Barber, D.L., Jayaraman, P., 2014. Orchestration of pulmonary T cell immunity during *Mycobacterium tuberculosis* infection: immunity interruptus. Semin. Immunol. 26:559–577. https://doi.org/10.1016/j.smim.2014.09.003.
Berry, M.P., Graham, C.M., Mcnab, F.W., Xu, Z., Bloch, S.A., Oni, T., Wilkinson, K.A., Banchereau, R., Skinner, J., Wilkinson, R.J., Quinn, C., Blankenship, D., Dhawan, R., Cush, J.J., Mejias, A., Ramilo, O., Kon, O.M., Pascual, V., Banchereau, J., Chaussabel, D., O'garra, A., 2010. An interferon-inducible neutrophil-driven blood transcriptional signature in human tuberculosis. Nature 466:973–977. https://doi.org/10.1038/nature09247.
Billeskov, R., Christensen, J.P., Aagaard, C., Andersen, P., Dietrich, J., 2013. Comparing adjuvanted H28 and modified vaccinia virus Ankara expressing H28 in a mouse and a non-human primate tuberculosis model. PLoS One 8. https://doi.org/10.1371/journal.pone.0072185.
Billeskov, R., Tan, E.V., Cang, M., Abalos, R.M., Burgos, J., Pedersen, B.V., Christensen, D., Agger, E.M., Andersen, P., 2016. Testing the H56 vaccine delivered in 4 different adjuvants as a BCG-booster in a non-human primate model of tuberculosis. PLoS One 11: e0161217. https://doi.org/10.1371/journal.pone.0161217.
Blair, D.A., Turner, D.L., Bose, T.O., Pham, Q.M., Bouchard, K.R., Williams, K.J., Mcaleer, J.P., Cauley, L.S., Vella, A.T., Lefrancois, L., 2011. Duration of antigen availability influences the expansion and memory differentiation of T cells. J. Immunol. 187:2310–2321. https://doi.org/10.4049/jimmunol.1100363.
Bryant, J.M., Harris, S.R., Parkhill, J., Dawson, R., Diacon, A.H., Van Helden, P., Pym, A., Mahayiddin, A.A., Chuchottaworn, C., Sanne, I.M., Louw, C., Boeree, M.J., Hoelscher, M., Mchugh, T.D., Bateson, A.L., Hunt, R.D., Mwaigwisya, S., Wright, L., Gillespie, S.H., Bentley, S.D., 2013. Whole-genome sequencing to establish relapse or re-infection with *Mycobacterium tuberculosis*: a retrospective observational study. Lancet Respir. Med. 1:786–792. https://doi.org/10.1016/S2213-2600(13)70231-5.
Busch, D.H., Frassle, S.P., Sommermeyer, D., Buchholz, V.R., Riddell, S.R., 2016. Role of memory T cell subsets for adoptive immunotherapy. Semin. Immunol. 28:28–34. https://doi.org/10.1016/j.smim.2016.02.001.
Cardoso, F.L., Antas, P.R., Milagres, A.S., Geluk, A., Franken, K.L., Oliveira, E.B., Teixeira, H.C., Nogueira, S.A., Sarno, E.N., Klatser, P., Ottenhoff, T.H., Sampaio, E.P., 2002. T-cell responses to the *Mycobacterium tuberculosis*-specific antigen ESAT-6 in Brazilian tuberculosis patients. Infect. Immun. 70, 6707–6714.
Caruso, A.M., Serbina, N., Klein, E., Triebold, K., Bloom, B.R., Flynn, J.L., 1999. Mice deficient in CD4 T cells have only transiently diminished levels of IFN-γ, yet succumb to tuberculosis. J. Immunol. 162, 5407–5416.
Cooper, A.M., Callahan, J.E., Keen, M., Belisle, J.T., Orme, I.M., 1997. Expression of memory immunity in the lung following re-exposure to *Mycobacterium tuberculosis*. Tuber. Lung Dis. 78, 67–73.
Counoupas, C., Pinto, R., Nagalingam, G., Britton, W.J., Petrovsky, N., Triccas, J.A., 2017. Delta inulin-based adjuvants promote the generation of polyfunctional CD4+ T cell responses and protection against *Mycobacterium tuberculosis* infection. Sci. Rep. 7: 8582. https://doi.org/10.1038/s41598-017-09119-y.
Crompton, J.G., Sukumar, M., Roychoudhuri, R., Clever, D., Gros, A., Eil, R.L., Tran, E., Hanada, K., Yu, Z., Palmer, D.C., Kerkar, S.P., Michalek, R.D., Upham, T., Leonardi, A., Acquavella, N., Wang, E., Marincola, F.M., Gattinoni, L., Muranski, P., Sundrud, M.S., Klebanoff, C.A., Rosenberg, S.A., Fearon, D.T., Restifo, N.P., 2015. Akt inhibition enhances expansion of potent tumor-specific lymphocytes with memory cell characteristics. Cancer Res. 75:296–305. https://doi.org/10.1158/0008-5472.CAN-14-2277.
De Boer, A.S., Van Soolingen, D., 2000. Recurrent tuberculosis due to exogenous reinfection. N. Engl. J. Med. 342, 1050–1051.
Dietrich, J., Roy, S., Rosenkrands, I., Lindenstrøm, T., Filskov, J., Rasmussen, E.M., Cassidy, J., Andersen, P., 2015. Differential influence of nutrient-starved mycobacterium tuberculosis on adaptive immunity results in progressive tuberculosis disease and pathology. Infect. Immun. 83:4731–4739. https://doi.org/10.1128/Iai.01055-15.
Fletcher, H.A., Snowden, M.A., Landry, B., Rida, W., Satti, I., Harris, S.A., Matsumiya, M., Tanner, R., O'shea, M.K., Dheenadhayalan, V., Bogardus, L., Stockdale, L., Marsay, L., Chomka, A., Harrington-Kandt, R., Manjaly-Thomas, Z.R., Naranbhai, V., Stylianou, E., Darboe, F., Penn-Nicholson, A., Nemes, E., Hatheril, M., Hussey, G., Mahomed, H., Tameris, M., Mcclain, J.B., Evans, T.G., Hanekom, W.A., Scriba, T.J., Mcshane, H., 2016. T-cell activation is an immune correlate of risk in BCG vaccinated infants. Nat. Commun. 7:11290. https://doi.org/10.1038/ncomms11290.
Gallegos, A.M., Van Heijst, J.W., Samstein, M., Su, X., Pamer, E.G., Glickman, M.S., 2011. A gamma interferon independent mechanism of CD4 T cell mediated control of *M. tuberculosis* infection in vivo. PLoS Pathog. 7:e1002052. https://doi.org/10.1371/journal.ppat.1002052.
Ghosh, S., Chackerian, A.A., Parker, C.M., Ballantyne, C.M., Behar, S.M., 2006. The LFA-1 adhesion molecule is required for protective immunity during pulmonary *Mycobacterium tuberculosis* infection. J. Immunol. 176, 4914–4922.
Green, A.M., Difazio, R., Flynn, J.L., 2013. IFN-γ from CD4 T cells is essential for host survival and enhances CD8 T cell function during *Mycobacterium tuberculosis* infection. J. Immunol. 190:270–277. https://doi.org/10.4049/jimmunol.1200061.
Guerra-Assuncao, J.A., Houben, R.M., Crampin, A.C., Mzembe, T., Mallard, K., Coll, F., Khan, P., Banda, L., Chiwaya, A., Pereira, R.P., Mcnerney, R., Harris, D., Parkhill, J., Clark, T.G., Glynn, J.R., 2015. Recurrence due to relapse or reinfection with *Mycobacterium tuberculosis*: a whole-genome sequencing approach in a large, population-based cohort with a high HIV infection prevalence and active follow-up. J. Infect. Dis. 211: 1154–1163. https://doi.org/10.1093/infdis/jiu574.
Henao-Tamayo, M., Obregon-Henao, A., Ordway, D.J., Shang, S.B., Duncan, C.G., Orme, I.M., 2012. A mouse model of tuberculosis reinfection. Tuberculosis 92:211–217. https://doi.org/10.1016/j.tube.2012.02.008.
Hoang, T., Aagaard, C., Dietrich, J., Cassidy, J.P., Dolganov, G., Schoolnik, G.K., Lundberg, C.V., Agger, E.M., Andersen, P., 2013. ESAT-6 (EsxA) and TB10.4 (EsxH) based vaccines for pre- and post-exposure tuberculosis vaccination. PLoS One 8:e80579. https://doi.org/10.1371/journal.pone.0080579.
Joosten, S.A., Van Meijgaarden, K.E., Del Nonno, F., Baiocchini, A., Petrone, L., Vanini, V., Smits, H.H., Palmieri, F., Goletti, D., Ottenhoff, T.H., 2016. Patients with tuberculosis have a dysfunctional circulating B-cell compartment, which normalizes following successful treatment. PLoS Pathog. 12:e1005687. https://doi.org/10.1371/journal.ppat.1005687.
Joshi, N.S., Cui, W., Chandele, A., Lee, H.K., Urso, D.R., Hagman, J., Gapin, L., Kaech, S.M., 2007. Inflammation directs memory precursor and short-lived effector CD8(+) T cell fates via the graded expression of T-bet transcription factor. Immunity 27: 281–295. https://doi.org/10.1016/j.immuni.2007.07.010.
Jung, Y.J., Ryan, L., Lacourse, R., North, R.J., 2005. Properties and protective value of the secondary versus primary T helper type 1 response to airborne *Mycobacterium tuberculosis* infection in mice. J. Exp. Med. 201:1915–1924. https://doi.org/10.1084/jem.20050265.
Kagina, B.M., Abel, B., Scriba, T.J., Hughes, E.J., Keyser, A., Soares, A., Gamieldien, H., Sidibana, M., Hatherill, M., Gelderbloem, S., Mahomed, H., Hawkridge, A., Hussey, G., Kaplan, G., Hanekom, W.A., Other Members of the South African Tuberculosis Vaccine, I, 2010. Specific T cell frequency and cytokine expression profile do not correlate with protection against tuberculosis after Bacillus Calmette-Guérin vaccination of newborns. Am. J. Respir. Crit. Care Med. 182:1073–1079. https://doi.org/10.1164/rccm.201003-0334OC.
Kamath, A.B., Behar, S.M., 2005. Anamnestic responses of mice following *Mycobacterium tuberculosis* infection. Infect. Immun. 73:6110–6118. https://doi.org/10.1128/IAI.73.9.6110-6118.2005.
Kauffman, K.D., Sallin, M.A., Sakai, S., Kamenyeva, O., Kabat, J., Weiner, D., Sutphin, M., Schimel, D., Via, L., Barry 3rd, C.E., Wilder-Kofie, T., Moore, I., Moore, R., Barber, D.L., 2017. Defective positioning in granulomas but not lung-homing limits CD4 T-cell interactions with *Mycobacterium tuberculosis*-infected macrophages in rhesus macaques. Mucosal Immunol. https://doi.org/10.1038/mi.2017.60.
Kawalekar, O.U., O'connor, R.S., Fraietta, J.A., Guo, L., Mcgettigan, S.E., Posey Jr., A.D., Patel, P.R., Guedan, S., Scholler, J., Keith, B., Snyder, N.W., Blair, I.A., Milone, M.C., June, C.H., 2016. Distinct signaling of coreceptors regulates specific metabolism pathways and impacts memory development in CAR T cells. Immunity 44:380–390. https://doi.org/10.1016/j.immuni.2016.01.021.
Keck, S., Schmaler, M., Ganter, S., Wyss, L., Oberle, S., Huseby, E.S., Zehn, D., King, C.G., 2014. Antigen affinity and antigen dose exert distinct influences on CD4 T-cell differentiation. Proc. Natl. Acad. Sci. U. S. A. 111:14852–14857. https://doi.org/10.1073/pnas.1403271111.
Klebanoff, C.A., Gattinoni, L., Torabi-Parizi, P., Kerstann, K., Cardones, A.R., Finkelstein, S.E., Palmer, D.C., Antony, P.A., Hwang, S.T., Rosenberg, S.A., Waldmann, T.A., Restifo, N.P., 2005. Central memory self/tumor-reactive CD8+ T cells confer superior antitumor immunity compared with effector memory T cells. Proc. Natl. Acad. Sci. U. S. A. 102: 9571–9576. https://doi.org/10.1073/pnas.0503726102.
Knudsen, N.P., Olsen, A., Buonsanti, C., Follmann, F., Zhang, Y., Coler, R.N., Fox, C.B., Meinke, A., D'oro, U., Casini, D., Bonci, A., Billeskov, R., De Gregorio, E., Rappuoli, R., Harandi, A.M., Andersen, P., Agger, E.M., 2016. Different human vaccine adjuvants promote distinct antigen-independent immunological signatures tailored to different pathogens. Sci. Rep. 6:19570. https://doi.org/10.1038/srep19570.
Kremer, L., Maughan, W.N., Wilson, R.A., Dover, L.G., Besra, G.S., 2002. The *M. tuberculosis* antigen 85 complex and mycolyltransferase activity. Lett. Appl. Microbiol. 34, 233–237.
Langermans, J.A., Doherty, T.M., Vervenne, R.A., Van Der Laan, T., Lyashchenko, K., Greenwald, R., Agger, E.M., Aagaard, C., Weiler, H., Van Soolingen, D., Dalemans, W., Thomas, A.W., Andersen, P., 2005. Protection of macaques against *Mycobacterium tuberculosis* infection by a subunit vaccine based on a fusion protein of antigen 85B and ESAT-6. Vaccine 23:2740–2750. https://doi.org/10.1016/j.vaccine.2004.11.051.
Lawn, S.D., Myer, L., Edwards, D., Bekker, L.G., Wood, R., 2009. Short-term and long-term risk of tuberculosis associated with CD4 cell recovery during antiretroviral therapy in South Africa. AIDS 23:1717–1725. https://doi.org/10.1097/QAD.0b013e32832d3b6d.
Leal, I.S., Smedegard, B., Andersen, P., Appelberg, R., 2001. Failure to induce enhanced protection against tuberculosis by increasing T-cell-dependent interferon-γ generation. Immunology 104, 157–161.
Lin, P.L., Dietrich, J., Tan, E., Abalos, R.M., Burgos, J., Bigbee, C., Bigbee, M., Milk, L., Gideon, H.P., Rodgers, M., Cochran, C., Guinn, K.M., Sherman, D.R., Klein, E., Janssen, C., Flynn, J.L., Andersen, P., 2012. The multistage vaccine H56 boosts the effects of BCG to protect cynomolgus macaques against active tuberculosis and reactivation of latent *Mycobacterium tuberculosis* infection. J. Clin. Invest. 122:303–314. https://doi.org/10.1172/JCI46252.
Lindenstrøm, T., Agger, E.M., Korsholm, K.S., Darrah, P.A., Aagaard, C., Seder, R.A., Rosenkrands, I., Andersen, P., 2009. Tuberculosis subunit vaccination provides long-term protective immunity characterized by multifunctional CD4 memory T cells. J. Immunol. 182:8047–8055. https://doi.org/10.4049/jimmunol.0801592.
Lindenstrøm, T., Woodworth, J., Dietrich, J., Aagaard, C., Andersen, P., Agger, E.M., 2012. Vaccine-induced Th17 cells are maintained long-term post-vaccination as a distinct and phenotypically stable memory subset. Infect. Immun. 80:3533–3544. https://doi.org/10.1128/Iai.00550-12.
Lindenstrøm, T., Knudsen, N.P.H., Agger, E.M., Andersen, P., 2013. Control of chronic *Mycobacterium tuberculosis* infection by CD4 KLRG1− IL-2-secreting central memory cells. J. Immunol. 190:6311–6319. https://doi.org/10.4049/jimmunol.1300248.
Lindestam Arlehamn, C.S., Gerasimova, A., Mele, F., Henderson, R., Swann, J., Greenbaum, J.A., Kim, Y., Sidney, J., James, E.A., Taplitz, R., Mckinney, D.M., Kwok, W.W., Grey, H., Sallusto, F., Peters, B., Sette, A., 2013. Memory T cells in latent *Mycobacterium tuberculosis* infection are directed against three antigenic islands and largely contained in a CXCR3+CCR6+ Th1 subset. PLoS Pathog. 9:e1003130. https://doi.org/10.1371/journal.ppat.1003130.

Luzze, H., Johnson, D.F., Dickman, K., Mayanja-Kizza, H., Okwera, A., Eisenach, K., Cave, M.D., Whalen, C.C., Johnson, J.L., Boom, W.H., Joloba, M., Tuberculosis Research, U., 2013. Relapse more common than reinfection in recurrent tuberculosis 1-2 years post treatment in urban Uganda. Int. J. Tuberc. Lung Dis. 17:361–367. https://doi.org/10.5588/ijtld.11.0692.

Marriott, C.L., Carlesso, G., Herbst, R., Withers, D.R., 2015. ICOS is required for the generation of both central and effector $CD4^+$ memory T-cell populations following acute bacterial infection. Eur. J. Immunol. 45:1706–1715. https://doi.org/10.1002/eji.201445421.

Moguche, A.O., Shafiani, S., Clemons, C., Larson, R.P., Dinh, C., Higdon, L.E., Cambier, C.J., Sissons, J.R., Gallegos, A.M., Fink, P.J., Urdahl, K.B., 2015. ICOS and Bcl6-dependent pathways maintain a CD4 T cell population with memory-like properties during tuberculosis. J. Exp. Med. 212:715–728. https://doi.org/10.1084/jem.20141518.

Moguche, A.O., Musvosvi, M., Penn-Nicholson, A., Plumlee, C.R., Mearns, H., Geldenhuys, H., Smit, E., Abrahams, D., Rozot, V., Dintwe, O., Hoff, S.T., Kromann, I., Ruhwald, M., Bang, P., Larson, R.P., Shafiani, S., Ma, S., Sherman, D.R., Sette, A., Lindestam Arlehamn, C.S., Mckinney, D.M., Maecker, H., Hanekom, W.A., Hatherill, M., Andersen, P., Scriba, T.J., Urdahl, K.B., 2017. Antigen availability shapes T cell differentiation and function during tuberculosis. Cell Host Microbe 21:695–706 (e5). https://doi.org/10.1016/j.chom.2017.05.012.

Mollenkopf, H.-J., Kursar, M., Kaufmann, S.H.E., 2004. Immune response to postprimary Tuberculosis in mice: *Mycobacterium tuberculosis* and *Mycobacterium bovis* bacille Calmette-Guérin induce equal protection. J. Infect. Dis. 190, 588–597.10.1086/422394.

Moon, J.J., Chu, H.H., Pepper, M., Mcsorley, S.J., Jameson, S.C., Kedl, R.M., Jenkins, M.K., 2007. Naive $CD4^+$ T cell frequency varies for different epitopes and predicts repertoire diversity and response magnitude. Immunity 27:203–213. https://doi.org/10.1016/j.immuni.2007.07.007.

Nandakumar, S., Kannanganat, S., Posey, J.E., Amara, R.R., Sable, S.B., 2014. Attrition of T-cell functions and simultaneous upregulation of inhibitory markers correspond with the waning of BCG-induced protection against tuberculosis in mice. PLoS One 9:e113951. https://doi.org/10.1371/journal.pone.0113951.

Orme, I.M., Robinson, R.T., Cooper, A.M., 2015. The balance between protective and pathogenic immune responses in the TB-infected lung. Nat. Immunol. 16:57–63. https://doi.org/10.1038/ni.3048.

Pepper, M., Pagan, A.J., Igyarto, B.Z., Taylor, J.J., Jenkins, M.K., 2011. Opposing signals from the Bcl6 transcription factor and the interleukin-2 receptor generate T helper 1 central and effector memory cells. Immunity 35:583–595. https://doi.org/10.1016/j.immuni.2011.09.009.

Petruccioli, E., Scriba, T.J., Petrone, L., Hatherill, M., Cirillo, D.M., Joosten, S.A., Ottenhoff, T.H., Denkinger, C.M., Goletti, D., 2016. Correlates of tuberculosis risk: predictive biomarkers for progression to active tuberculosis. Eur. Respir. J. 48:1751–1763. https://doi.org/10.1183/13993003.01012-2016.

Prota, G., Christensen, D., Andersen, P., Medaglini, D., Ciabattini, A., 2015. Peptide-specific T helper cells identified by MHC class II tetramers differentiate into several subtypes upon immunization with CAF01 adjuvanted H56 tuberculosis vaccine formulation. Vaccine 33:6823–6830. https://doi.org/10.1016/j.vaccine.2015.09.024.

Reiley, W.W., Shafiani, S., Wittmer, S.T., Tucker-Heard, G., Moon, J.J., Jenkins, M.K., Urdahl, K.B., Winslow, G.M., Woodland, D.L., 2010. Distinct functions of antigen-specific CD4 T cells during murine *Mycobacterium tuberculosis* infection. Proc. Natl. Acad. Sci. U. S. A. 107:19408–19413. https://doi.org/10.1073/pnas.1006298107.

Rogerson, B.J., Jung, Y.J., Lacourse, R., Ryan, L., Enright, N., North, R.J., 2006. Expression levels of *Mycobacterium tuberculosis* antigen-encoding genes versus production levels of antigen-specific T cells during stationary level lung infection in mice. Immunology 118:195–201. https://doi.org/10.1111/j.1365-2567.2006.02355.x.

Rosenthal, I.M., Tasneen, R., Peloquin, C.A., Zhang, M., Almeida, D., Mdluli, K.E., Karakousis, P.C., Grosset, J.H., Nuermberger, E.L., 2012. Dose-ranging comparison of rifampin and rifapentine in two pathologically distinct murine models of tuberculosis. Antimicrob. Agents Chemother. 56:4331–4340. https://doi.org/10.1128/AAC.00912-12.

Sackstein, R., Schatton, T., Barthel, S.R., 2017. T-lymphocyte homing: an underappreciated yet critical hurdle for successful cancer immunotherapy. Lab. Investig. 97:669–697. https://doi.org/10.1038/labinvest.2017.25.

Sakai, S., Kauffman, K.D., Schenkel, J.M., Mcberry, C.C., Mayer-Barber, K.D., Masopust, D., Barber, D.L., 2014. Cutting edge: control of *Mycobacterium tuberculosis* infection by a subset of lung parenchyma-homing CD4 T cells. J. Immunol. 192:2965–2969. https://doi.org/10.4049/jimmunol.1400019.

Sakai, S., Kauffman, K.D., Sallin, M.A., Sharpe, A.H., Young, H.A., Ganusov, V.V., Barber, D.L., 2016. CD4 T cell-derived IFN-γ plays a minimal role in control of pulmonary *Mycobacterium tuberculosis* infection and must be actively repressed by PD-1 to prevent lethal disease. PLoS Pathog. 12:e1005667. https://doi.org/10.1371/journal.ppat.1005667.

Sallin, M.A., Sakai, S., Kauffman, K.D., Young, H.A., Zhu, J., Barber, D.L., 2017. Th1 differentiation drives the accumulation of intravascular, non-protective CD4 T cells during tuberculosis. Cell Rep. 18:3091–3104. https://doi.org/10.1016/j.celrep.2017.03.007.

Scanga, C.A., Mohan, V.P., Joseph, H., Yu, K., Chan, J., Flynn, J.L., 1999. Reactivation of latent tuberculosis: variations on the Cornell murine model. Infect. Immun. 67, 4531–4538.

Schluns, K.S., Lefrancois, L., 2003. Cytokine control of memory T-cell development and survival. Nat. Rev. Immunol. 3:269–279. https://doi.org/10.1038/nri1052.

Scriba, T.J., Carpenter, C., Pro, S.C., Sidney, J., Musvosvi, M., Rozot, V., Seumois, G., Rosales, S.L., Vijayanand, P., Goletti, D., Makgotlho, E., Hanekom, W., Hatherill, M., Peters, B., Sette, A., Arlehamn, C.S.L., 2017. Differential recognition of *Mycobacterium tuberculosis*-specific epitopes as a function of Tuberculosis disease history. Am. J. Respir. Crit. Care Med. 196:772–781. https://doi.org/10.1164/rccm.201706-1208OC.

Sheridan, B.S., Lefrancois, L., 2011. Regional and mucosal memory T cells. Nat. Immunol. 12, 485–491.

Shi, L., North, R., Gennaro, M.L., 2004. Effect of growth state on transcription levels of genes encoding major secreted antigens of *Mycobacterium tuberculosis* in the mouse lung. Infect. Immun. 72:2420–2424. https://doi.org/10.1128/iai.72.4.2420-2424.2004.

Sonnenberg, P., Murray, J., Glynn, J.R., Shearer, S., Kambashi, B., Godfrey-Faussett, P., 2001. HIV-1 and recurrence, relapse, and reinfection of tuberculosis after cure: a cohort study in south African mineworkers. Lancet 358:1687–1693. https://doi.org/10.1016/s0140-6736(01)06712-5.

Srivastava, S., Ernst, J.D., 2013. Cutting edge: direct recognition of infected cells by CD4 T cells is required for control of intracellular *Mycobacterium tuberculosis* in vivo. J. Immunol. 191:1016–1020. https://doi.org/10.4049/jimmunol.1301236.

Tameris, M.D., Hatherill, M., Landry, B.S., Scriba, T.J., Snowden, M.A., Lockhart, S., Shea, J.E., Mcclain, J.B., Hussey, G.D., Hanekom, W.A., Mahomed, H., Mcshane, H., Team, M.A.T.S., 2013. Safety and efficacy of MVA85A, a new tuberculosis vaccine, in infants previously vaccinated with BCG: a randomised, placebo-controlled phase 2b trial. Lancet 381:1021–1028. https://doi.org/10.1016/S0140-6736(13)60177-4.

Taylor, J.L., Bielefeldt-Ohmann, H., Pozzi, A., Izzo, A.A., 2008. Lack of α-1 integrin alters lesion morphology during pulmonary *Mycobacterium tuberculosis* infection. Tuberculosis (Edinb) 88:444–452. https://doi.org/10.1016/j.tube.2008.05.006.

Torrado, E., Fountain, J.J., Liao, M., Tighe, M., Reiley, W.W., Lai, R.P., Meintjes, G., Pearl, J.E., Chen, X., Zak, D.E., Thompson, E.G., Aderem, A., Ghilardi, N., Solache, A., Mckinstry, K.K., Strutt, T.M., Wilkinson, R.J., Swain, S.L., Cooper, A.M., 2015. Interleukin 27Rf regulates CD4 + T cell phenotype and impacts protective immunity during *Mycobacterium tuberculosis* infection. J. Exp. Med. 212:1449–1463. https://doi.org/10.1084/jem.20141520.

Uys, P., Brand, H., Warren, R., Van Der Spuy, G., Hoal, E.G., Van Helden, P.D., 2015. The risk of tuberculosis reinfection soon after cure of a first disease episode is extremely high in a hyperendemic community. PLoS One 10:e0144487. https://doi.org/10.1371/journal.pone.0144487.

Verver, S., Warren, R.M., Beyers, N., Richardson, M., Van Der Spuy, G.D., Borgdorff, M.W., Enarson, D.A., Behr, M.A., Van Helden, P.D., 2005. Rate of reinfection tuberculosis after successful treatment is higher than rate of new tuberculosis. Am. J. Respir. Crit. Care Med. 171:1430–1435. https://doi.org/10.1164/rccm.200409-1200OC.

Weng, N.P., Araki, Y., Subedi, K., 2012. The molecular basis of the memory T cell response: differential gene expression and its epigenetic regulation. Nat. Rev. Immunol. 12:306–315. https://doi.org/10.1038/nri3173.

Woodworth, J.S., Aagaard, C.S., Hansen, P.R., Cassidy, J.P., Agger, E.M., Andersen, P., 2014. Protective CD4 T cells targeting cryptic epitopes of *Mycobacterium tuberculosis* resist infection-driven terminal differentiation. J. Immunol. 192:3247–3258. https://doi.org/10.4049/jimmunol.1300283.

Woodworth, J.S., Cohen, S.B., Moguche, A.O., Plumlee, C.R., Agger, E.M., Urdahl, K.B., Andersen, P., 2016. Subunit vaccine H56/CAF01 induces a population of circulating CD4 T cells that traffic into the *Mycobacterium tuberculosis*-infected lung. Mucosal Immunol. https://doi.org/10.1038/mi.2016.70.

Zak, D.E., Penn-Nicholson, A., Scriba, T.J., Thompson, E., Suliman, S., Amon, L.M., Mahomed, H., Erasmus, M., Whatney, W., Hussey, G.D., Abrahams, D., Kafaar, F., Hawkridge, T., Verver, S., Hughes, E.J., Ota, M., Sutherland, J., Howe, R., Dockrell, H.M., Boom, W.H., Thiel, B., Ottenhoff, T.H., Mayanja-Kizza, H., Crampin, A.C., Downing, K., Hatherill, M., Valvo, J., Shankar, S., Parida, S.K., Kaufmann, S.H., Walzl, G., Aderem, A., Hanekom, W.A., Acs & Groups, G. C. C. S., 2016. A blood RNA signature for tuberculosis disease risk: a prospective cohort study. Lancet 387:2312–2322. https://doi.org/10.1016/S0140-6736(15)01316-1.